Glacier area change (1993-2019) and its relationship to debris cover, proglacial lakes, and morphological parameters in the Chandra-Bhaga Basin, Western Himalaya, India

VATSAL Sarvagya[1,5]* https://orcid.org/0000-0003-4576-0778; e-mail: sarvagyavatsaljnu@gmail.com

AZAM Mohd Farooq[1] https://orcid.org/0000-0002-4176-9807; e-mail: farooqazam@iiti.ac.in

BHARDWAJ Anshuman[2] https://orcid.org/0000-0002-2502-6384; e-mail: anshuman.bhardwaj@abdn.ac.uk

MANDAL Arindan[3] https://orcid.org/0000-0003-1616-6032; e-mail: arindan141@gmail.com

BAHUGUNA Ishmohan[4] https://orcid.org/0000-0001-8651-6849; e-mail: imbisro@gmail.com

RAMANATHAN Alagappan[5] https://orcid.org/0000-0002-3491-2273; e-mail: alrjnu@gmail.com

RAJU N. Janardhana[5] https://orcid.org/0000-0001-7330-461X; e-mail: rajunj7@gmail.com

TOMAR Sangita Singh[6] https://orcid.org/0000-0003-0633-5250; e-mail: singh.sangita15@gmail.com

**Corresponding author*

1 Department of Civil Engineering, Indian Institute of Technology Indore, Simrol 453552, India
2 School of Geosciences, University of Aberdeen, King's College, Aberdeen AB24 3FX, United Kingdom
3 Interdisciplinary Centre for Water Research, Indian Institute of Science, Bengaluru 560012, India
4 Space Application Centre, Ahmedabad 380015, India
5 School of Environmental Sciences, Jawaharlal Nehru University, New Delhi 110067, India
6 Department of Geography, Norwegian University of Science and Technology, Trondheim No-7491, Norway

Abstract: Glacier inventories serve as critical baseline data for understanding the impacts of climate change on glaciers. The present study maps the outlines of glaciers in the Chandra-Bhaga Basin (western Himalaya) for the years 1993, 2000, 2010, and 2019 using Landsat Thematic Mapper (TM), Enhanced Thematic Mapper (ETM), and Operational Land Imager (OLI) datasets. A total of 251 glaciers, having an area of > 0.5 km², were identified, which include 216 clean-ice and 35 debris-covered glaciers. Area changes are estimated for three periods: 1993-2000, 2000-2010, and 2010-2019. The total glacierized area was 996 ± 62 km² in 1993, which decreased to 973 ± 70 km² in 2019. The mean rate of glacier area loss was higher in the recent decade (2010-2019), at 0.036 km², compared to previous decades (0.029 km² in 2000-2010 and 0.025 km² in 1993-2000). Supraglacial debris cover changes are also mapped over the period of 1993 and 2019. It is found that the supraglacial debris cover increased by 14.1 ± 2.54 km² (15.2%) during 1993-2019. Extensive field surveys on Chhota Shigri, Panchi II, Patsio, Hamtah, Mulkila, and Yoche Lungpa glaciers were carried out to validate the glacier outlines and supraglacial debris cover estimated using satellite datasets. Controls of various morphological parameters on retreat were also analyzed. It is observed that small, clean ice, south oriented glaciers, and glaciers with proglacial lakes are losing area at faster rates than other glaciers in the basin.

Keywords: Glacier; Area change; Debris cover; Morphology; Proglacial lake

1 Introduction

Himalayan, Karakoram, and Hindukush (HKH) are home to vast quantities of cryospheric elements, including snow and glaciers, which are major sources of fresh water in the region (Bolch et al. 2019). The meltwater from the snow and glaciers of the HKH mountain ranges, combined with rain and groundwater, serves as the source of fresh water that flows into the three rivers and their tributaries: the Indus, Ganges, and Brahmaputra. These perennial rivers support the livelihoods of over a billion people residing in mountainous regions and low-lying plains by meeting their agricultural practices, hydropower generation, and domestic water requirements (Azam et al. 2021). Therefore, it is crucial to periodically monitor the frozen resources of fresh water in the HKH region, especially considering the impact of climate change on these water reserves and the potential occurrence of cryosphere-related risks including Glacier Lake Outburst Floods (GLOFs), and floods that could exert substantial socio-economic repercussions in the region (Azam et al. 2018; Kulkarni et al. 2021; Andermann et al. 2023). The periodic monitoring of such a vast cryospheric reserve is only possible through the utilization of remotely sensed datasets and glacier modelling at different spatial scales (Tawde et al. 2017; Farinotti et al. 2019; Muhammad and Thapa 2020; Srivastava et al. 2022). The remote-sensing datasets have been extensively used in snow cover mapping (Rathore et al. 2022), generation of glacier inventories in cryospheric regions (Schmidt and Nüsser 2017; Muhammad and Thapa 2020), as well as geodetic mass balance estimation (Shean et al. 2020; Hugonnet et al. 2021).

Glacier inventories play a crucial role as a foundational reference for evaluating the effects of climate change on glacier mass balance and dynamics (Haeberli and Hoelzle 1995). Glacier inventories comprise mapping glacier outlines and their morphological characteristics, such as aspect, area, slope, elevation, etc., using satellite images and Digital Elevation Models (DEMs). These inventories provide essential information for estimating geodetic mass balances (Shean et al. 2020), hydrological modelling (Bliss and Hock 2014), glacier volume (Farinotti et al. 2019), and surface velocity (Dehecq and others, 2019) as well as geohazard assessment (Shugar et al. 2021; Sattar et al. 2023).

Various studies have examined the challenges in obtaining reliable glacier inventories (Racoviteanu et al. 2009, 2019; Paul et al. 2017; Sakai 2019), and identified diffrences in glacier outlines of the various inventories such as the RGI (RGI Consortium 2017), GAMDAM (Sakai 2019), and ICIMOD (Barjacharya and Shrestha 2011), which are extensively used for the glacier studies (Mölg et al. 2018; Sakai 2019). The primary reasons for these inconsistencies are as follows: 1) data availability, ensuring no interference from cloud cover; 2) steep accumulation areas of glaciers; 3) attached snow fields, dead ice, rock glaciers; 4) drainage location derived from the DEM; 5) different time periods for which the glacier inventories have been developed; and 6) Surface Debris Cover (SDC), which presents a significant hurdle in compiling glacier outlines (Paul et al. 2013; Mölg et al. 2018), especially in the western Himalaya, where debris cover constitutes approximately 21% of the total glacier area (Scherler et al. 2011a). Besides debris cover, complex geomorphology of the Himalayan glaciers further adds to the uncertainty in glacier delineation (Bhambri and Bolch 2009; Bhardwaj et al. 2014).

Despite numerous constraints associated with using satellite images, extensive work has been conducted on glacier mapping in the HKH region utilizing optical satellite images such as Landsat and Sentinel (Kulkarni et al. 2007; Sakai 2019; Shukla et al. 2020; Bahuguna et al. 2021). The variations observed in these inventories can be ascribed to the aforementioned challenges in addition to other factors, such as spatial resolution of the dataset, time period considered, automated approaches used for glacier delineation, and the delineation of basin and sub-basin boundaries. The utilization of an automated approach for glacier delineation in the Himalaya introduces uncertainties due to the SDC and complex geomorphology characterizing glaciers in the region (Bhambri et al. 2011; Huang et al. 2021).

Numerous studies have extensively investigated glacier area changes of the Chandra and Bhaga basin glaciers. Pandey and Venkataraman (2013) reported a 2.5% area loss for 15 glaciers in the Chandra-Bhaga Basin between 1980 and 2010. Expanding their scope, Kulkarni et al. (2011) estimated area changes for 116 glaciers in Chandra and 111 glaciers in the Bhaga Basin between 1962 and 2001/2004, revealing area losses of 30% and 20% for Chandra and Bhaga basins' glaciers, respectively during the same period. Patel et al. (2021) extended this analysis to 67 and 102 glaciers in Bhaga and Chandra basins, estimating area losses of 14.7% and 5.6%, respectively, between 1971 and 2018. Sahu and Gupta (2020) reported a 4.9% area loss between 1971 and 2016 for 169 the glaciers in the Chandra Basin. They also described the role of morphological factors in glacier change, but their focus was limited to Chandra Basin glaciers. Garg et al. (2017) focused only on three glaciers in the Chandra Basin: Chhota Shigri, Sakchum, and Bara Shigri, reporting area losses of 1.26%, 3.17%, and 0.92%, respectively, between 1993 and 2014. Another study by Birajdar et al. (2014) reported a 1.63% loss of glacier area for the 231 glaciers in the Bhaga Basin.

Despite the extensive studies on glaciers in the Chandra-Bhaga Basin, a multi-decadal area change analysis including all glaciers is still lacking, supported by extensive fieldwork surveys. In addition to glacier area change estimation, it is crucial to understand the factors influencing area changes on glaciers in the basin. A significant gap remains in understanding areal changes on every glacier (area > 0.5 km^2) in the Chandra-Bhaga Basin and comprehending the role of morphological factors and proglacial lakes on the areal changes of these glaciers. Furthermore, SDC quantification on every glacier in the Chandra-Bhaga Basin has not been addressed yet. Extensive fieldwork for validating glacier outlines and SDC is notably lacking in previous studies focused on glaciers in the Chandra-Bhaga Basin. Addressing these challenges, the objectives of the present study are to extend the current knowledge about the Chandra-Bhaga Basin by 1) estimating the multitemporal glacier area change for three periods: 1993-2000, 2000-2010, and 2019-2019 2) producing an SDC dataset using field datasets, and 3) analysing the influence of geomorphic features (glacier size, slope, elevation, SDC, and aspect) and proglacial lakes on spatiotemporal glacier changes.

2 Study Area

The Chandra-Bhaga Basin is located in the Lahaul-Spiti district in Himachal Pradesh (western Himalaya), India (Fig. 1). The Chandra and Bhaga rivers, two sub-basins of Chandra-Bhaga Basin, meet at Tandi village and then flow as the Chenab River (Fig. 1). A total of 17 large hydropower projects are proposed within the Chenab Basin. Among these, the Chhatu, Seli, Sachkhas, and Purthi projects are specifically reliant on the discharge from the Chandra and Bhaga rivers (Sandrp 2023). Manali is the nearest town to the Chandra-Bhaga Basin.

The climate of this region is governed by the Western Disturbances during winter and the Indian Summer Monsoon during summer (Bookhagen and Burbank 2010). Nearly 70% of annual precipitation in this sub-basin occurs in the form of snowfall in winter, while 30% falls during summer; therefore, the region is characterized as the monsoon-arid transition zone (Mandal et al. 2020). Chhota Shigri (Mandal et al. 2020; Srivastava and Azam 2022), Sutri Dhaka (Oulkar et al. 2022), Hamtah (Kumar et al. 2016), and Patsio (Angchuk et al. 2021) are the most studied glaciers in the Chandra-Bhaga Basin.

3. Data and Methodology

3.1 Dataset

Various satellite datasets from different years have been used in the present study for glacier boundary delineation (Appendix 1). Landsat data rectified at the L1 processing level (radiometrically corrected and orthorectified) were used for the glacier outline delineation. While SRTM DEM was used for basin boundary delineation. Additionally, very-high resolution images from Google Earth and field surveys photographs were used to delineate the glacier boundary, especially in the accumulation zone. In two instances, specifically for the years 1993 and 2010, we encountered challenges with obtaining a cloud-free dataset (less than 15%) for certain regions of the basin. Consequently, we opted to utilize datasets from 1992 and 2011 for those respective years for certain regions. RGI 6.0 (RGI Consortium 2017) and GAMDAM (Sakai 2019) were used for the comparison with our delineated glacier outlines in the Chandra-Bhaga Basin.

3.2 Glacier outline delineation

Different methods for glacier boundary delineation, such as band rationing and thresholding (Paul et al. 2004), supervised classification, and the Normalized Difference Snow Index (NDSI) have been used for delineation (Gratton et al. 1990; Aniya et al. 1996; Sidjak and Wheate 1999; Racoviteanu et al. 2008) of the glaciers. Delineation of debris-covered glaciers poses a significant challenge due to the complex nature of their surfaces. Numerous studies have addressed this challenge by exploring automated delineation methods, including those based on NDSI and Band ratio techniques (Bhardwaj et al. 2014; Mölg et al. 2018; Holobâcă et al. 2021). Despite these efforts, distinguishing the precise extent of debris-covered glacier ice remains problematic, primarily attributed to the similar spectral signatures exhibited by the glacier's surrounding debris (Bhambri and Bolch 2009). In the present study, all the glaciers with an area > 0.5 km^2 have been manually delineated, which include both clean-ice and debris-covered glaciers. The primary rationale for adopting a threshold of 0.5 km^2 was to mitigate potential uncertainties arising from glacier size variability, which has been estimated to be ~12 to 15% for glaciers with an area less than 0.5 km^2 (Soheb et al. 2022). It has been assumed that the upper boundary of glaciers has not changed significantly (Bhambri et al. 2011). The snouts of all glaciers, encompassing both clean ice and debris-covered portions, were identified through meticulous visual inspection. This process involved focusing on the stream's origin point and discerning the shadow cast by the ice wall. The glacier outlines for clean ice as well as debris-covered glaciers were subsequently digitized manually through visual interpretation of the satellite dataset.

The major challenges for glacier delineation are: 1) debris cover, 2) cloud cover, 3) snow cover, and 4) shadow. Debris cover on the glacier is primarily a result of the steep topography that intermittently deposits debris onto the glacier through rockfalls/avalanches (Scherler et al. 2011b; Herreid et al. 2015). Debris-covered glaciers can be identified based on certain features such as a thin debris cover (< 1 m), large melt-out depressions (thermokarst), supraglacial lakes, and a chaotic hummocky surface (Bodin et al. 2010). Another challenge is the small solar incidence angle at higher altitudes, which minimizes topographic contrast around the terminus of the glacier. To counter these challenges, manual digitization becomes imperative, ensuring minimum error and better accuracy (Kulkarni et al. 2007; Bhambri and Bolch 2009). To this end, Google Earth imagery was used to further delineate the glacier boundary (Mölg et al. 2018). Minimal interference from cloud cover (less than 15%) was ensured. To minimize the snow cover related errors, multiple datasets were downloaded for peak ablation season, viz. June, July, August, September, and October. All the datasets were analyzed, and only the images with minimum snow cover on the glacier surface were selected. Another challenge is mountain shadows, which decrease the reflectance values. This is a significant problem in high-altitudes regions. To counter these problems, different bands of Landsat were used, and better results were obtained in the blue band (0.45- 0.51 μm) of Landsat (Paul et al. 2002). Further, as highlighted earlier, Google Earth imagery was also used to improve the accuracy of dataset. For the estimation of glacier area change, the final area was subtracted from the initial area over the specified study duration.

3.2.1 Uncertainty related to glacier delineation

There are primarily three types of uncertainties associated with glacier delineation. Firstly, the uncertainty of manually digitized glacier outline which is a fixed uncertainty (Mölg et al. 2018). Secondly, the uncertainty determined by the input image's spatial resolution, which is calculated with the buffer-based estimate (Granshaw and Fountain 2006; Bolch et al. 2010). Another source of uncertainty is related to the workload associated with the manual digitization of the glaciers (Paul et al. 2017). This type of uncertainty arises due to the multi-temporal digitization of glaciers, stemming from the tiredness of analysts involved in the digitization process (Paul et al. 2017; Mölg et al. 2018).

To address all these sources of uncertainty, we first estimated fixed uncertainty of manually digitized glacier outline, which is ± 2% and ± 5% of glacier area for clean ice and debris-covered glaciers, respectively, as an upper boundary estimate, while excluding the overlap between the two surface types (Paul et al. 2011, 2013). Next, we estimated the buffer method uncertainty (Granshaw and Fountain 2006) with ± 1/2 pixel and ± 1 pixel for clean-ice and debris-covered glaciers, respectively (Mölg et al. 2018). Lastly, to enhance overall accuracy and quantify the uncertainty related to workload, we performed multiple digitization of the glaciers to estimate uncertainty. Furthermore, we conducted comprehensive field surveys on glaciers, including Chhota Shigri, Panchi II, Mulkila, Yoche Lungpa, Patsio, and Hamtah, to validate the glacier boundaries and termini positions manually digitized based on satellite datasets in this study. Additional details regarding these field surveys can be found in Section 3.4.

3.2.2 Uncertainty of the area change

Uncertainty in area change was estimated using the following equation (Hall et al. 2003; Wang et al. 2009):

$$U_{area} = 2 \times U_{retreat} \times V \tag{1}$$

Here U_{area} is the uncertainty in the area change estimation, $U_{retreat}$ is the uncertainty in the area estimation, and V is the image pixel resolution.

3.3 Supraglacial debris cover estimation

For the estimation of the SDC, unsupervised classification, supervised classification, normalized difference snow index (NDSI) and principal component analysis (PCA) techniques have been used in previous studies (Aniya et al. 1996; Sidjak and Wheate 1999; Kääb 2002; Racoviteanu et al. 2008). However, to avoid any confusion between SDC and proglacial debris, we exclusively employed the supervised maximum likelihood classification (MLC) method (Gratton et al. 1990) within the delineated glacier extent. We relied on the MLC because this method is well established for the Himalayan glaciers with an accuracy of ~ 94 % to 98 % (Yan et al. 2014), when calculated by ArcGIS software. MLC was also tested for the glaciers in the Chandra-Bhaga Basin, resulting in an accuracy range of 82% to 95% for estimating SDC (Shukla et al. 2009). Specifically, we utilized band 2 (green), 3 (red), and 4 (NIR) for

Landsat 5 (TM) and band 3 (green), 4 (red), and 5 (NIR) for Landsat 8 (OLI) to estimate the SDC. By employing the same frequency bands as the previous study (Shukla et al. 2009), we aimed to ensure consistency and comparability in our analysis. In the MLC, a pixel is classified based on its likelihood of belonging to a specific class, which is described by the mean and covariance of a normal distribution in the space of multispectral features. For the classification process, we generated four training samples, namely snow, ice, ice mixed debris, and debris. These training samples were based on the field surveys done on the selected glaciers of the Chandra-Bhaga Basin. A detailed discussion of these training samples is provided in the subsequent section, 3.3.1. Landsat dataset for the year 1993 and 2019 were used to estimate the SDC change (Appendix 1).

3.3.1 Accuracy assessment of MLC method for SDC estimation

The confusion matrix, derived from the image map and classified data, was generated for accuracy assessment (Janssen and van der Wel 1994). The coefficient of agreement between the classified image and ground reference data was calculated using Kappa (Ismail and Jusoff 2008). The Kappa value ranges between 0 and 1, with 1 indicating complete agreement between the two datasets and 0 indicating agreement due to chance alone (Fitzgerald and Lees 1994). Equations (2) and (3) quantify accuracy and Kappa coefficient.

$$\text{Overall accuracy} = \frac{\text{Total number of correctly classified pixels}}{\text{Total number of reference pixels}} \quad (2)$$

$$\text{Kappa coefficient} = \frac{(\text{TS}\times\text{TCS})-(\sum \text{Column total}\times\text{Row total})}{\text{TS}^2 - \sum(\text{Column total}-\text{Row total})} \quad (3)$$

where TS = total sample, TCS = total correctly classified samples, Column total, and Row total refer to sum of columns and rows in the Table 1 for each respective class.

To ensure high accuracy of the MLC, on-field visual inspection is essential (Paul 2000). A total of 154 ground observation points were sampled and compared to the remotely classified satellite imagery of Chhota Shigri, Patsio, Panchi II, Mulkila, Hamtah, and Yoche Lungpa glaciers (Fig. 2, Table 1). 70% of these ground observations (107) were used to train the remote classification, while 30% (47) were used to evaluate the accuracy of remotely classified Landsat dataset. The ground observations covered the entire range from the glacier snout up to the accumulation zone. The presence of debris, ice, ice mixed debris, and snow was recorded during these surveys using a Garmin eTrex 30X GPS, with a team of three co-authors involved in the data collection process. Further information, including specific survey dates, is elaborated in Section 3.4.

3.4 Field survey for glacier outline

Rigorous field surveys were conducted on the following glaciers: Hamtah in August 2017, Chhota Shigri in August 2019, Patsio in August 2019, Mulkila in June 2017, Yoche Lungpa in June 2017, and Panchi II in August 2019. It was observed that Mulkila, Yoche Lungpa, Hamtah, and Panchi II glaciers have a significant amount of SDC (Fig. 2).

During our field surveys, we also measured the termini/snout position of all the glaciers using a handheld Garmin eTrex 30X GPS, which has a position accuracy of ± 3 m. We also conducted surveys of the lateral moraines of the glaciers, which are one of the major sources of uncertainty in identifying the boundaries of debris-covered glaciers as discussed in section 3.2. The inclusion of these two surveys (termini and moraines) enhances the accuracy of our glacier boundary outline dataset (Fig. 2).

In addition, we conducted surveys of the accumulation areas of Chhota Shigri, Hamtah, Panchi II, and Patsio glaciers to enhance the accuracy of the glacier boundary delineation in the accumulation zone and to assess any uncertainties related to avalanches in boundary identification (Fig. 2). To minimize the uncertainty arising from the time difference between the satellite scenes used in the study, we ensured that the scenes fell within a maximum time gap of ± 1 year from the target year (Appendix 1) as mentioned in section 3.1. This approach aids in mitigating potential uncertainties associated with the temporal gap between the satellite images (Mölg et al. 2018).

3.5 DEM and its derivatives

SRTM DEMs have been utilized extensively for glacier-related studies (Berthier et al. 2016; Brun et al. 2017; Mukherjee et al. 2018; Ramsankaran et al. 2018; Shean et al. 2020; Hugonnet et al. 2021). We utilized the SRTM DEM (Appendix 1) to estimate the elevation range, aspect, and slope of the delineated glaciers in the present study. These datasets were employed to assess the influence of these morphological factors on the area change of glaciers in the Chandra-Bhaga Basin.

3.6 Proglacial lakes

Proglacial lakes within the Chandra-Bhaga Basin were identified through manual analysis of Google Earth imagery using QGIS. Special attention was given to confirming the presence of these proglacial lakes for both the years 1993 and 2019. This thorough verification was conducted to comprehensively assess the influence of proglacial lakes on the area changes observed for glaciers within the Chandra-Bhaga Basin.

3.7 Linear analysis Multivariate Linear model

In the univariate linear analysis, we implemented multivariate linear model, a statistical model used to analyze the relationship between multiple independent variables (glacier size, minimum elevation, slope, aspect, and SDC) and a single dependent variable (Area change between 1993-2019). The Multivariate linear models determine which independent variables have a significant influence on the dependent variable, and the relative contribution of each independent variable. The equation for multivariate linear regression is:

$$Y = \beta_0 + \beta_1 X_1 + \beta_2 X_2 + \ldots + \beta_n X_n + \varepsilon \quad (4)$$

Where: Y is the dependent variable, β_0 is the intercept, β_1 to β_n are the coefficients for the independent variables X_1 to X_n, respectively, X_1 to X_n are the independent variables, ε is the residual error

The standard approaches used for model selection, such as forward selection and backward elimination (Akaike 1974), involve evaluating the model by adding or removing variables until an optimal combination is reached to remove redundant variables (minimum elevation, SDC, and aspect) (Hocking 1976).

3.8 Climate data

The climate dataset used in this study includes the fifth generation of the European Reanalysis (ERA5) 2m air temperature (Hersbach et al. 2020) and Indian Meteorological Department (IMD) precipitation data (Pai et al. 2014). ERA5 is a global atmospheric reanalysis dataset produced by the European Centre for Medium-Range Weather Forecasts (ECMWF). It provides hourly estimates of various meteorological variables, such as temperature, pressure, wind speed, and precipitation, at a spatial resolution of 0.25 degrees. In addition to ERA5 data, the study also incorporates precipitation data from the IMD. The IMD provides detailed information on daily precipitation at a spatial resolution of 0.25 degrees.

4 Results and Discussion

4.1 Morphological characteristics of glaciers

We identified 251 glaciers larger than 0.5 km² in the Chandra-Bhaga Basin. The glacierized area for 251 outlined glaciers ranges from 0.5 to 131.3 km², with an average glacier area of 3.5 km². Only 58 glaciers had an area greater than 3.5 km², indicating a prevalence of smaller-sized glaciers in the sub-basins. Out of the 251 outlined glaciers, 42 glaciers range in area from 3.5 km² to 10 km², while only 16 glaciers have an area > 10 km². Bara Shigri is the largest glacier in the basin, with an area of 131.3 ± 9.5 km², followed by Samudra Tapu and Mulkila glaciers with areas of 81.7 ± 5.1 and 30.7 ± 2.5 km², respectively. There are a total of 71 north-facing glaciers, 31 northeast-facing glaciers, 32 east-facing glaciers, 25 southeast-facing glaciers, 37 south-facing glaciers, 21 southwest facing glaciers, 15 west-facing glaciers, and 19 northwest-facing glaciers. These represent the principal directions of the glaciers in the Chandra-Bhaga Basin. The glaciers' slopes in the basin vary from 9° to 36°, with a mean slope of 18.7°. Variation in the mean elevation for the glaciers ranges from 4148 to 5678 m a.s.l., with a mean elevation of 5211 m a.s.l. Debris cover on the glacier varies from 0 to 62%, relative to the entire glacier area. A threshold of 15% or more has been considered to qualify a glacier to be called as debris-covered glacier in the Chandra-Bhaga Basin (Xiang et al. 2018; Brun et al. 2019), and based on these criteria, a total of 35 debris-covered glaciers have been identified in our study. A total of 11 proglacial lakes have been identified, with five lakes associated with clean glaciers and six lakes associated with debris-covered glaciers.

4.2 Uncertainty of glacier outline

Cumulative fixed uncertainties estimated for all the glaciers in the basin ranged between ± 27 km^2 and ± 29 km^2 (2% of total glacier area), while the cumulative uncertainty estimated for all the glaciers in the basin using the buffer method ranged between ± 62 km^2 and ± 70 km^2 (6% total glacier area). The mean fixed uncertainty ranges from 0.11 km^2 to 0.12 km^2, whereas the mean uncertainty using the buffer method ranges between 0.25 km^2 and 0.28 km^2. To address the possibility of double-counting uncertainty in areas where neighboring glaciers overlap, particularly within the buffer zone, where accumulation zones overlap, we implemented a unified approach to uncertainty assessment for these glacier complexes (Mölg et al. 2018). Additionally, multiple digitization was conducted, resulting in a ± 4% standard deviation (averaged over all experiments). This high value highlights the mapping challenges in the Himalaya caused by cloud cover, SDC, shadows, and snow cover. We evaluated the uncertainty in the digitization of small glaciers (less than 1 km^2) that had a significant portion of their surface shrouded in shadow and a considerable portion covered in barely traceable SDC and found it to be ± 6% of the glacier area mapped. Such cases are extremely rare in our database and have no bearing on the level of uncertainty. It has been reported previously that analyst interpretation for debris-covered glaciers and glacier parts in shadow can differ up to 50% (Paul et al. 2013, 2015). In addition, we quantified the uncertainty of the glacier outlines through field surveys conducted on Chhota Shigri, Patsio, and Panchi II glaciers in the year 2019, as detailed in Section 3.4. The uncertainties for the glacier outlines in 2019 were determined as 0.02 km^2, 0.008 km^2, and 0.03 km^2, respectively, for Chhota Shigri, Patsio, and Panchi II glaciers, respectively. These uncertainties were notably lower compared to other sources of quantified uncertainties for the same glaciers. In the present study, we find that for such glaciers manual digitization is favorable.

4.3 Glacier area change

The total area of 251 glaciers decreased from 996 ± 62 km^2 in 1993 to 973 ± 70 km^2 in 2019, an area shrinkage of 23 ± 8 km^2, equivalent to 0.09% $year^{-1}$. To understand the rate of changes in area of glaciers, the time span of 27 years has been split into three intervals: 1993-2000, 2000-2010, and 2010-2019. In year 2000, the area was mapped as 989 ± 68 km^2, and in 2010 it was mapped as 982 ± 66 km^2 (Table 2). The mean area loss per glacier in the first interval was observed as 0.025 ± 0.001 km^2, in second interval as 0.029 ± 0.001 km^2, and in third interval as 0.036 ± 0.002 km^2. The total mean area loss was 0.09 ± 0.002 km^2 between 1993-2019. Table 3 presents the decadal area changes for 13 glaciers as mentioned in Fig. 1. Additionally, Fig. 3 illustrates the area change near the snout of Hamtah, Chhota Shigri, Samudra Tapu, Batal, Mulkila, and Panchi I glaciers. Of these, Panchi I and Samudra Tapu glaciers have a lake at their snout.

4.4 Comparison with RGI and GAMDAM glacier outline

We compared the outlines of selected glaciers within the Chandra-Bhaga Basin (Fig. 1) to those outlined in the RGI 6.0 (RGI consortium 2017) and GAMDAM (Sakai 2019) inventories (Fig. 4). Several issues related to the gap area, differences in mapping methods, and skill of the analysts involved lead to misrepresentation and limit the accuracy of inventories. For example, RGI 6.0 (RGI consortium 2017) and GAMDAM (Sakai 2019) overestimate parts of the extent in some glaciers including, Chhota Shigri (Fig. 4B), Gepang Gath (Fig. 4D), Panchi I (Fig. 4E), and Sutri Dhaka (Fig. 4K) glaciers, while underestimating for others, such as Batal (Fig. 4H), Bara Shigri (Fig. 4A), and Panchi II (Fig. 4F). The total glacier area estimated using our glacier outline is approximately 26% and 9% lower compared to the RGI 6.0 and GAMDAM (Sakai 2019) inventories, respectively. It has been observed previously that the RGI 6.0 inventory has overestimated glacier area by ~100 % in the North Patagonian Andes (Zalazar et al. 2020), ~10 % in China (Li et al. 2022), and ~14 % for Ladakh region (Soheb et al. 2022), which may be attributed to uncertainties associated with the misinterpretation of seasonal snow cover and SDC (Pfeffer et al. 2014). Another potential factor could be the methodology used and absence of glacier changes over time, possibly arising from the utilization of imagery captured over a broad span of acquisition years employed in creating RGI 6.0 and GAMDAM inventories. The present study is centered on a smaller spatial scale i.e., Chandra-Bhaga Basin only, enabling the generation of more precise glacier outlines. Additionally, it offers glacier outlines at various temporal scales, which represents a significant advantage over the RGI and GAMDAM inventories. This improved approach yields enhanced accuracy in glacier delineation and provides valuable insights into glacier area change over time for the glaciers in the Chandra-Bhaga Basin.

4.5 Supraglacial debris cover change

We have compiled an up-to-date dataset of the debris cover for glaciers in the Chandra-Bhaga Basin, delineated for the years 1993 and 2019. This dataset represents a comprehensive compilation that quantifies the changes in SDC in the Chandra-Bhaga Basin. Total SDC in the Chandra-Bhaga Basin was estimated to be 91.4 ± 16.4 km^2 in 1993, which increased to 105.5 ± 18.9 km^2 in 2019, indicating a total increase of 14.1 ± 2.54 km^2 over the study period. Table 4 entails the SDC changes for some representative glaciers (marked in Fig. 1) in the basin. We highlighted the changes in SDC for the Chhota Shigri, Sakchum, and Bara Shigri glaciers (Fig. 5). It is evident that in 2019, a distinct medial moraine and debris cover on the eastern flank is prominently visible on the Chhota Shigri Glacier. On the other hand, for the Sakchum and Bara Shigri glaciers, the presence of SDC has increased, and SDC is more visible towards the accumulation zone of the glaciers (Fig. 5), which agrees with the study by Garg et al. (2017).

In a previous study conducted on the 185 glaciers in the Chandra-Bhaga Basin, it was estimated that there was an increase in SDC of approximately 1.83 ± 1.6 km^2 between 1994 and 2009 (Gaddam et al. 2016). The observed increase in SDC estimated by Gaddam et al. (2016) was comparatively lower than our findings. This discrepancy can be attributed to differences in temporal scale and the number of glaciers under observation in both the studies. The present study specifically focuses on SDC changes for 251 glaciers over the period 1993-2019. In contrast, Gaddam et al. (2016) assessed SDC changes for a smaller set of 185 glaciers, limited to the period between 1994 and 2009. The study conducted by Garg et al. (2017) focused on specific glaciers within the Chandra-Bhaga Basin, namely Chhota Shigri, Sakchum, and Bara Shigri glaciers. They estimated the SDC change on Chhota Shigri, Sakchum, and Bara Shigri glaciers as 0.5 km^2, 1.0 km^2, and 4.8 km^2, respectively, between 1993 and 2014. Their findings align with our research, indicating an observed increase in SDC on these selected glaciers.

The increase in SDC on the Chandra-Bhaga Basin glaciers can be attributed to multiple factors, including continuous glacier melting (Shean et al. 2020; Mandal et al. 2020; Angchuk et al. 2021) over the past few decades. The melting of glaciers has resulted in the exposure of lateral and medial moraines, which have contributed debris to the surface of the glacier. Furthermore, snow and rock avalanches serve as direct sources of debris on the glacier surface. During the field survey of Panchi II and Chhota Shigri glaciers, our observations revealed occurrences of both rock and snow avalanches on these glaciers. The continuous supply of rocks was observed originating from the lateral walls, depositing onto the glacier surface through these avalanches. It has also been reported previously that glaciers located in valleys with steep walls that facilitate a continuous supply of debris through avalanches are more likely to exhibit higher debris cover (Garg et al. 2017).

4.6 Uncertainty in debris cover estimation

The overall accuracy of MLC classification was found to be 90% (based on eq. 2 and Table 1). The individual accuracies for debris, ice, snow, and ice mix with debris were 95%, 90%, 94%, and 82%, respectively. These accuracy values are remarkably high, considering the intricate geomorphology of the glaciers in the Chandra-Bhaga Basin. The Kappa value of 0.87 (estimated using eq. 3 and Table 1) indicates a strong agreement between the remotely classified image and the ground validation points (Table 1). The maximum uncertainty was found to be approximately 18% for the class "ice mix with debris." To ensure the accuracy of our estimate, we assigned this value as the uncertainty in the SDC area estimation using MLC. As a result, the total uncertainty in SDC was ± 16.4 km^2 in 1993 and ± 18.9 km^2 in 2019.

4.7 Factors governing glacier dimensional change

In this section we investigated the role of morphological parameters (glacier size, slope, elevation, SDC, aspect, and proglacial lake) on the estimated glacier area changes.

4.7.1 Impact of glacier size

It is interesting to note that all glaciers with an area loss > 20% are clean ice glaciers with an area < 2 km^2. The influence of glacier area is clearly evident on glaciers with an area < 5 km^2, as the number of glaciers with an area < 1 km^2 increased from 62 to 72 during the period of study, while the number of glaciers with an area > 5 km^2 remained the same. Taking this into consideration, we made glacier classes using 5 km^2 glacier area intervals. However, large glaciers also retreated, albeit at a smaller rate as compared to smaller glaciers. In Fig. 6a, the columns represent the mean percentage of area change for different glacier area classes (0-5, 5-10…, 30-35 km^2) during different time periods. The analysis shows that the mean area change is higher for small glaciers, with the highest change observed in the area class of 0-5 km^2, throughout the period of 1993-2019. The changes are most prominent during the recent decade of 2010-2019 as compared to previous decades. Previous studies in other regions have reported that small glaciers have deglaciated at a faster rate than larger glaciers. Bhambri et al. (2011) found a higher rate of area loss for small glaciers (< 1 km^2) than large glaciers between 1968 to 2006 in the Garhwal Himalaya. A similar trend was observed for glaciers in the Miyar Basin (Patel et al. 2018). The higher shrinkage of smaller glaciers is probably due to higher mass wastage, as the smaller glaciers are more sensitive to changing climate (Paul et al. 2002; Jin et al. 2005).

4.7.2 Impact of SDC

The effect of presence of SDC in minimizing glacier area loss is evident from the scatterplot (Fig. 6a). Due to the majority of glaciers in the Chandra-Bhaga Basin having an area below 4 km^2 (mean glacier area in 1993), we have categorized them into classes (Fig. 6a) based on their size to better comprehend the influence of SDC on spatiotemporal changes. The area change is higher in case of clean ice glaciers (max = 27.86%) compared to debris-covered glaciers (max = 16.44%). Similarly, in case of larger glaciers (> 4 km^2), excluding Samudra Tapu and Bara Shigri glaciers, we find clean ice glaciers (max = 5.38%) underwent greater area change than debris-covered glaciers (max = 4.23%). Total glacier area for clean ice (debris-covered) glaciers was 702.4 ± 38 km^2 (293.9 ± 25 km^2) in 1993 and decreased to 682 ± 36 km^2 (290.3 ± 25 km^2) in 2019. Also, the mean glacier area for clean ice (debris-covered) glaciers changed from 3.3 (8.16) km^2 in 1993 to 3.17 (8.06) km^2 in 2019. Despite their comparatively smaller numbers, mean glacier area of the debris-covered glaciers is greater than clean-ice glaciers, which shows greater variability in case of debris-covered glaciers (Standard deviation, σ = 21.62) compared to clean-ice glaciers (σ = 6.81). While comparing individual debris-covered glaciers with adjacent clean-ice glaciers of similar orientation, it has been observed that clean-ice glaciers have lost more area (Fig. 7). For instance, Sutri Dhaka and Batal are adjacent glaciers having same orientation (No. 6 and 5 in Fig. 1), and Batal Glacier covered with debris (27% SDC) showed less area loss than clean-ice Sutri Dhaka Glacier (Table 5, Fig. 7). Similarly, among Chhota Shigri and Sakchum glaciers (adjacent glaciers with similar orientation, No. 3 and 2 in Fig. 1), Chhota Shigri is considered a clean-ice glacier, with only 12% of its total surface area covered by debris at its snout (Table 5). Its area loss was greater than the Sakchum Glacier, which has 24% of its surface area covered by the debris. Similar results were obtained on comparing Patsio (clean ice) and Panchi II (debris-covered) glaciers having similar orientation (No. 13 and 11 in Fig. 1), where area loss for the Patsio Glacier is higher than Panchi II Glacier (Table 5, Fig. 7).

It is evident that debris-covered glaciers are experiencing a slower rate of shrinkage compared to clean-ice glaciers. Similar findings have been observed in the other parts of the Himalaya (Scherler et al. 2011b; Basnett et al. 2013; Shukla and Qadir 2016; Bahuguna et al. 2021). Generally, debris-covered glaciers have a gentle slope in their ablation area and an avalanche-fed accumulation part (Herreid et al. 2015). Such gentle slope reduces glacier velocity to a minimum at the terminus, affecting glacier retreat (Scherler et al. 2011a). Apart from this, ice loss near the terminus of the debris-covered glaciers is minimal because of debris pressure, which compacts the ice, preventing detachment from the glaciers' surface, thereby minimizing the retreat (Salerno et al. 2017).

4.7.3 Impact of elevation

Fig. 6b shows the glacier area change with respect to glacier elevation. In the Chandra-Bhaga Basin, glacier elevation (Z) ranges from 3533 to 5374 m a.s.l., and the mean minimum elevation is 4797 m a.s.l. In the minimum elevation range of Z < 5000 m (Z > 5000 m), 44% (13%) of all glaciers have an area change of < 5%, whereas 4.3% (7.2%) have an area change > 10% between 1993-2019. The mean elevation for the clean ice glaciers was 5251 m a.s.l., while for the debris-covered glaciers it was 4956 m a.s.l. We observed that the snout elevation of most debris-covered glaciers is lower compared to that of clean-ice glaciers. The present study aimed to examine the role of minimum elevation (snout elevation) on glacier shrinkage, but no definitive relationship was found. These findings are consistent with previous studies conducted in the Chandra-Bhaga Basin (Das and Sharma 2019). In addition, similar to the present study, several previous studies on the Himalayan glaciers have also reported no significant relationship between altitude and glacier area change (Chand and Sharma 2015; Salerno et al. 2017; Zhao et al. 2020; Patel et al. 2021).

4.7.4 Impact of slope

Glaciers with an area larger (smaller) than the mean glacier area of 4 km^2 had mean slope of 16° (20°). Irrespective of the elevation range, steeper slopes correspond to greater area change (Fig. 6b), which is also reported previously in the Chandra-Bhaga Basin (Pandey and Venkataraman 2013) and in Warwan-Bhut region, which is a part of Chenab Basin (Brahmabhatt et al. 2017). The glaciers' average slope varies in different areas; for example, the accumulation area is steep for all glaciers while debris-covered areas have gentle slope. This observation suggests that the influence of individual factors, such as slope, on the retreat of glaciers is not distinctly evident.

4.7.5 Impact of aspect

Glacier area change is maximum (> 25%) for glaciers facing south (southwest - southeast) (SW - SE), as seen in Fig. 6c. Average area loss for south (north) facing glaciers was 0.11 ± 0.007 km^2 (0.08 ± 0.004 km^2). However, the highest area change (27.86%) corresponds to an east facing glacier, which can be attributed to the presence of a proglacial lake at the snout. We observed that, excluding the lake terminating glaciers, generally in Chandra-Bhaga Basin glaciers having south, southeast, and southwest orientations are shrinking faster than the other glaciers having other aspects (Fig. 6c). In agreement, in the Jankar Chhu watershed, it has been observed that south facing glaciers are retreating faster than other glaciers (Das and Sharma 2019). Similar findings have been observed in various regions, such as the Sagarmatha National Park region, the Kanchenjunga-Sikkim area, and the Baspa Basin in the western Himalaya, where south-facing glaciers have been observed to retreat at a faster rate (Salerno et al. 2008; Racoviteanu et al. 2015). This may be attributed to less solar radiation availability for the north facing glaciers. Various studies state that south facing glaciers, even in complex local topography, are more likely to receive more solar heat, available for glacier melting, thereby accelerating retreat (Fujita and Ageta 2000; Oliphant et al. 2003; Azam et al. 2014).

4.7.6 Impact of proglacial lakes

A total of 11 glaciers with proglacial lakes have been identified. Out of these, 9 were associated with clean-ice and 2 with debris-covered glaciers. The total area loss for these 11 glaciers was 2.03 ± 0.42 km^2 between 1993 and 2019, with a mean area loss of 0.19 ± 0.006 km^2 per glacier. This is higher compared to the mean area loss for glaciers without proglacial lakes, which is 0.08 ± 0.002 km^2. In the case of Panchi II and Panchi I glaciers, which have similar SDC and glacier size, it is notable that only Panchi I Glacier features a lake at its snout. The observed area loss between 1993 and 2019 for Panchi II Glacier was estimated to be 0.06 ± 0.001 $km^2 year^{-1}$, while for Panchi I Glacier, the area loss was measured at 0.10 ± 0.001 $km^2 year^{-1}$, which exemplifies the effect of the proglacial lake on the glacier area change.

Calving is an important component of mass loss of a glacier terminating into proglacial lakes (Sakai et al. 2009; Maurer et al. 2016). The heat absorption by the proglacial lake water is mostly responsible for the glacier mass loss at the snout, contributing towards higher snout retreat (Bolch et al. 2012; King et al. 2018). Such a high percentage of area loss is significant, making such glaciers vulnerable to changing climate and a threat to downstream communities through possible GLOF. For example, Gepang Gath Glacier's proglacial lake poses an important risk, given that it is expected to significantly increase in size, and an associated GLOF could have a severe impact on communities downstream (Sattar et al., 2023).

4.8 Heterogeneity in retreat

Glaciers are intricate systems influenced by a multitude of morphological parameters, including elevation, slope, aspect, size, and SDC, as previously discussed. While each of these parameters may individually contribute to the dynamics of a glacier, comprehending their combined impact on spatiotemporal changes can be challenging. Relying solely on a single morphological parameter may be inadequate for explaining the observed spatiotemporal changes in glaciers within the Chandra-Bhaga Basin.

Considering a combination of morphological parameters provides a more holistic perspective on the factors influencing glacier area changes. For example, glaciers at lower elevations tend to experience greater area loss compared to those at higher elevations due to the influence of higher temperatures. However, the retreat of glaciers at lower elevations can be attenuated by the presence of SDC, which acts as an insulating layer. This insulation effect can potentially slow down the rate of retreat in these lower elevation glaciers.

4.8.1 Heterogeneous nature of glaciers due to morphological parameters

It has been found that SDC, slope, elevation, and avalanche explain a maximum 8% of glacier mass balance variability (Brun et al. 2017) in Lahaul- Spiti region of the western Himalaya. We have also quantified the role of the SDC, glacier size, minimum elevation, slope, and aspect on the spatiotemporal changes between 1993 and 2019 for the Chandra-Bhaga Basin glaciers. It has been found that aspect, SDC, and minimum elevation are not good predictors of spatiotemporal changes on the Chandra-Bhaga Basin glaciers in comparison to the size and slope of the glaciers. Glacier size has a negative correlation ($r = -0.002$, $p < 0.05$) with area loss of the glaciers, while slope also follows the same trend ($r = -0.12$, $p < 0.05$). The multivariate linear model was able to explain 12% of the variability of spatiotemporal change on the glacier of the Chandra-Bhaga Basin. This means that the two variables (glacier size and slope) taken together could explain 12% of the observed changes in glacier area (Table 6). However, it's important to note that this model does not consider any interaction between the variables, it only assumes a linear relationship between each variable and the area change.

4.9 Climatic control

The present study employed statistical tests, including the Mann-Kendall and Sen's slope test, on the annual mean temperature and precipitation datasets, with a confidence interval of 95%. The results indicate an overall increase in temperature and a decrease in rainfall over the three decades (Fig. 8A and B). Specifically, temperature has increased by approximately 0.032° C $year^{-1}$ between 1960 and 2019. These findings align with the trends observed by Kaushik et al. (2020), who reported an annual mean temperature increase at the rate of 0.027° C $year^{-1}$ (1961-2015) in the Bhaga Basin. In contrast, precipitation has shown a decreasing trend. It decreased by a rate of -0.074 mm $year^{-1}$ between 1960 and 2019. Additionally, Garg et al. (2023) conducted a climate trend analysis for the period 1983-2016 using a meteorological station located at Patsio in the Bhaga Basin at an elevation of 3800 m a.s.l. They observed a decrease in maximum annual precipitation between 2008-2016 (73 cm), compared to 1983-1989 (102 cm) and 2000-2008 (94 cm). The persistent rise in temperature, coupled with a reduction in precipitation, has significantly intensified the melting of glacier snow and ice. Consequently, this heightened melting has led to an escalation in the mass loss of the glaciers. These climatic changes have exerted a pronounced influence on glacier dynamics, markedly impacting the rate of glacier area loss.

4.10 Comparison with previous studies for the region

It is worth noting that there is a scarcity of high-quality datasets and limited comprehensive studies in the Chandra-Bhaga Basin. Moreover, differences in time periods, datasets, and methodologies among these studies make it difficult to conduct a thorough comparison. However, previous research in the region has shown a decline in glacierized areas. Pandey and Venkataraman (2013) reported a 2.5% decrease in glacier area in the Chandra-Bhaga Basin over a 30-year period from 1980 to 2010, which is similar to the 2.3% area loss identified in our study. Glacier area in the year 2000 for the selected representative glaciers by Pandey and Venkataraman, (2013), (373.1 km^2) and present study (374.64 km^2) are also in agreement. Glacier area in 2000 from the present study was found comparable with the area estimated for year 2002 by Sahu and Gupta (2020), with respect to 5 glaciers they chose for a detailed analysis, namely: Gepang Gath (12.7 and 13.40 km^2), Samudra Tapu (80.8 and 81.9 km^2), Bara Shigri (125.1 and 131.5 km^2), Chhota Shigri (14.0 and 15.88 km^2) and Hamtah (3.4 and 3.8 km^2) respectively. Garg et al. (2017) studied 3 glaciers during 1993-2014. Area in 1993 for these glaciers namely: Sakchum (15.61 km^2), Chhota Shigri (15.22 km^2), and Bara Shigri (127.63 km^2), as well as our estimates of 16.04 ± 1.63 km^2, 15.88 ± 0.85 km^2, and 131.50 ± 9.56 km^2 respectively, are within a comparable range. It can be suggested that the reason for the lower estimation of the Bara Shigri Glacier area in the studies conducted by Garg et al. (2017) and Sahu and Gupta (2020) is the exclusion of the glacier's flanks. These flanks contribute to the overall glacier flux and have been considered in several other studies (Chand et al. 2017; Yellala et al. 2019; Nela et al. 2020).

The distinctions in glacier boundary defined by different studies contribute further to the challenge of statistical intercomparison and necessitates field surveys and visual inspection in order to ensure accuracy. Therefore, we have carried out various field surveys while also accounting for the following challenges: 1) Nature of the dataset used in the studies: For example, Pandey and Venkataraman (2013) used Landsat MSS and AWiFS dataset having resolution of 80 and 56 m, respectively, and co-registration error of 13 and 24 m. The present study has attempted to account for these uncertainties in the glacier inventory by improving on the spatial resolution (viz. Pan sharped Landsat 15 m), and consequently observed a comparatively lesser rate of glacier area loss. 2) Different methodologies for glacier boundary delineation: While the majority are clean-ice glaciers, several representative glaciers within the study region are debris-covered, making it difficult to differentiate SDC from the surrounding topography (Bolch et al. 2008). The automated approach to delineate glacier boundary has more uncertainty in comparison to the manual approach (Bhambri and Bolch, 2009). Manual digitization carried out in the present study reduces uncertainty as compared to other studies that have opted for a semi-automated approach (viz. Sahu and Gupta 2020). This is highlighted above by the example of the difference in the area of the Bara Shigri Glacier.

The SDC area estimation conducted in this study is comparable to the results of Garg et al. (2017) for three specific glaciers. For instance, the estimated SDC change between 1993 and 2019 for Sakchum was 1.0 ± 0.18 km^2 in this study, while Garg et al. (2017) reported it as 1.03 km^2. Similarly, the estimated SDC change for Chhota Shigri was 0.71 ± 0.13 km^2 in this study, whereas Garg et al. (2017) reported it as 0.45 km^2. For Bara Shigri, the estimated SDC change was 4.94 ± 0.89 km^2 in this study and 4.82 km^2 by Garg et al. (2017). It is important to note that our study includes a larger dataset, covering 251 glaciers in the Chandra-Bhaga Basin.

5 Conclusions

In the present study, we provided two types of datasets of glaciers in the Chandra-Bhaga Basin, western Himalaya, which quantify spatiotemporal changes between 1993-2019. These datasets include: 1) a homogenous, multitemporal (1993, 2000, 2010, 2019) glacier outline, and 2) SDC on each glacier for years 1993 and 2019. Major constraints (snow cover, cloud cover, SDC, and hill shade) have been addressed by selecting Landsat images from the ablation season with minimum cloud and snow cover and digitization based on visualization interpretation. For the SDC estimation, we have performed MLC within the glacier outlines boundary generated in present study, followed by extensive field surveys (with a total of 39 ground validation points for SDC) to enhance the accuracy of the dataset.

We mapped 251 glaciers with area > 0.5 km^2, which include 216 clean-ice and 35 debris-covered glaciers. Eleven glaciers with proglacial lake were identified. Total glacierized area showed a continuous reduction: 996 ± 62 km^2 in 1993, 989 ± 68 km^2 in 2000, 982 ± 66 km^2 in 2010, and 973 ± 70 km^2 in 2019. The multitemporal glacier area change further reveals valuable information regarding the impact of morphological factors on glacier area change in the Chandra-Bhaga Basin: 1) debris-covered glaciers are shrinking at a lesser rate compared to clean-ice glaciers, 2) south facing glaciers are losing comparatively more area than other aspects, 3) elevation does not play any significant role, and 4) land-terminating glaciers are more stable than glaciers having proglacial lake. It has also been observed that these factors operate simultaneously, contributing to the heterogeneous spatio-temporal changes in glacier areas within the region. Furthermore, the statistical analysis indicates that the combined influence of glacier size and slope could explain 12% of the observed changes in glacier area. SDC cover mapping for the years 1993 and 2019 shows that debris cover has increased by 14.1 ± 2.54 km^2 during 1993-2019.

The spatiotemporal data of glacier outlines and debris cover generated in this study will aid in future research endeavors focusing on glacio-hydrological and policy-based studies, as well as contribute towards improving existing inventory information's at both local and regional scales. Also, constant monitoring of glaciers, and further studies into the associated feedback processes is deemed necessary considering the excessive dependence of the downstream population on these glaciers, and the increasing demand for freshwater resources. The dataset produced in this study serves as a valuable resource for other researchers, enabling them to estimate and gain insights into the dynamics of glaciers in the Chandra-Bhaga Basin.

Acknowledgements

We are grateful to the Space Application Center, Ahmedabad (ISRO) for providing field support under "Integrated studies of Himalayan Cryosphere" program. We also extend our gratitude to the Glaciology Group, Jawaharlal Nehru University for providing necessary support for this research. MFA acknowledges the grants from SERB (CRG/2020/004877) and MOES/16/19/2017-RDEAS projects. SV and MFA express appreciation for the support from ISRO/RES/4/690/21-22 project.

Author contribution

VATSAL Sarvagya, BHARDWAJ Anshuman, MANDAL Arindan, and AZAM Mohd Farooq conceptualized the study. VATSAL Sarvagya and MANDAL Arindan carried out the field work and analysis. VATSAL Sarvagya wrote the manuscript with the inputs from BHARDWAJ Anshuman, RAMANATHAN Alagappan, MANDAL Arindan, AZAM Mohd Farooq, BAHUGUNA Ishmohan, RAJU N. Janardhana, and TOMAR Sangita Singh.

Ethics Declaration

Data Availability: The dataset used in the study is available in the appendix part of the manuscript in tabular form (Appendix 1). All the datasets including: 1) inventory of 251 glaciers (> 0.5 km^2) for 1993, 2000, 2010, and 2019; 2) debris cover area for year 1993 and 2019 are available on the Zenodo portal (https://doi.org/10.5281/zenodo.6595546).

Conflict of interest: The authors declare no conflict of interest.

References

Akaike H (1974) A new look at statistical model identification. IEEE Trans Autom control 19(6): 716-723. https://doi.org/10.1109/TAC.1974.1100705

Andermann C, Nepal S, Wagnon P, et al. (2023) Glaciers and glacier lake outburst flood. Himalaya, dynamics of a Giant 3: Current activity of Himalayan range. Willey International Publishing. pp 55-93.

Angchuk T, Ramanathan A, Bahuguna IM, et al. (2021) Annual and seasonal glaciological mass balance of Patsio Glacier, western Himalaya (India) from 2010 to 2017. J Glaciol 67(266): 1137-1146. https://doi.org/10.1017/jog.2021.60

Aniya M, Sato H, Naruse R, et al. (1996) The use of satellite and airborne imagery to inventory outlet glaciers of the Southern Patagonia Icefield, South America. Photogramm Eng Remote Sens 62(12):1361–1369.

Azam MF, Wagnon P, Berthier, et al. (2018) Review of the status and mass changes of Himalayan-Karakoram glaciers. J. Glaciol 64(243):61–74. https://doi.org/doi:10.1017/jog.2017.86

Azam MF, Kargel JS, Shea JM, et al. (2021) Glaciohydrology of the Himalaya-Karakoram. Science 373(6557) 3668:eabf3668. https://doi.org/10.1126/science.abf3668

Azam MF, Wagnon P, Patrick C, et al (2014) Reconstruction of the annual mass balance of Chhota Shigri glacier, western Himalaya, India, since 1969. Ann Glaciol 55(66):69–80. https://doi.org/10.3189/2014AoG66A104

Barjacharya, SR, Shrestha, B (2011) The status of glaciers in the Hindu Kush–Himalayan region. Kathmandu: ICIMOD. pp1–127. https://doi.org/10.53055/ICIMOD.551

Bahuguna I, Rathore BP, Jasrotia AS, et al. (2021) Recent glacier area changes in Himalaya–Karakoram and the impact of latitudinal variation. Curr Sci 121:929–940. https://doi.org/10.18520/CS/V121/I7/929-940

Basnett S, Kulkarni AV, Bolch T (2013) The influence of debris cover and glacial lakes on the recession of glaciers in Sikkim Himalaya, India. J Glaciol 59(218):1035–1046. https://doi.org/10.3189/2013JoG12J184

Berthier E, Cabot V, Vincent C, et al. (2016) Decadal region-wide and glacier-wide mass balances derived from multi-temporal aster satellite digital elevation models. Validation over the mont-blanc area. Front Earth Sci 4:1–16. https://doi.org/10.3389/feart.2016.00063

Bhambri R, Bolch T (2009) Glacier mapping: a review with special reference to the Indian Himalayas. Prog Phys Geogr 33(5):672–704. https://doi.org/10.1177/0309133309348112

Bhambri R, Bolch T, Chaujar RK, et al. (2011) Glacier changes in the Garhwal Himalaya, India, from 1968 to 2006 based on remote sensing. J Glaciol 57(203):543–556. https://doi.org/10.3189/002214311796905604

Bhardwaj A, Kumar P, Kumar M, et al. (2014) Mapping debris-covered glaciers and identifying factors affecting the accuracy. Cold Reg Sci Technol 106–107:161–174. https://doi.org/10.1016/j.coldregions.2014.07.006

Birajdar F, Venkataraman G, Bahuguna I, et al. (2014) A revised glacier inventory of Bhaga Basin Himachal Pradesh, India: current status and recent glacier variations. ISPRS Ann. Photogramm. Remote Sens. Spatial Inf. Sci II-8: 37–43. https://doi.org/10.5194/isprsannals-II-8-37-2014

Bliss A , Hock R, Radic V (2014) Global response of glacier runoff to twenty-first century climate change. J Geophys Res Earth Surf 119(4):717-730. https://doi.org/10.1002/2013JF002931

Bodin X, Rojas F, Brenning A (2010) Status and evolution of the cryosphere in the Andes of Santiago (Chile, 33.5°S.). Geomorphology 118(3-4):453–464. https://doi.org/10.1016/j.geomorph.2010.02.016

Bolch T, Buchroithner M, Pieczonka T, et al. (2008) Planimetric and volumetric glacier changes in the Khumbu Himal, Nepal, since 1962 using Corona, Landsat TM and ASTER data. J Glaciol 54(187):592–600. https://doi.org/10.3189/002214308786570782

Bolch T, Kulkarni A, Kääb A, et al (2012) The state and fate of Himalayan glaciers. Science 336(6079):310–314. https://doi.org/10.1126/science.121582

Bolch T, Yao T, Kang S, et al (2010) A glacier inventory for the western Nyainqentanglha range and the Nam Co Basin, Tibet, and glacier changes 1976-2009. The Cryosphere 4(3):419–433. https://doi.org/10.5194/tc-4-419-2010

Bolch T, Joseph MS, Shiyin L, et al. (2019) Status and change of the cryosphere in the extended Hindu Kush Himalaya region. The Hindu Kush Himalaya Assessment- Mountains, Climate Change, Sustainability and People. Springer International Publishing, Cham: pp 209–255. https://doi.org/10.1007/978- 3-319-92288-1

Bookhagen B, Burbank DW (2010) Toward a complete Himalayan hydrological budget: Spatiotemporal distribution of snowmelt and rainfall and their impact on river discharge. J Geophys Res Earth Surf 115(F3):1–25. https://doi.org/10.1029/2009JF001426

Brahmabhatt R, Bahuguna IM, Rathore BP, et al. (2017) Significance of glacio morphological factors in glacier retreat : a case study of part of Chenab basin, Himalaya. J Mt Sci 14:128–141. https://doi.org/10.1007/s11629-015-3548-0

Brun F, Berthier E, Wagnon P, et al. (2017) A spatially resolved estimate of High Mountain Asia glacier mass balances from 2000 to 2016. Nat Geosci 10:668–673. https://doi.org/10.1038/ngeo2999

Brun F, Wagnon P, Berthier E, et al. (2019) Heterogeneous influence of glacier morphology on the mass balance variability in High Mountain Asia. J Geophys Res Earth Surf 124(6):1331–1345. https://doi.org/10.1029/2018JF004838

Chand P, Sharma MC (2015) Glacier changes in the Ravi basin, North-Western Himalaya (India) during the last four decades (1971-2010/13). Glob Planet Change 135:133–147. https://doi.org/10.1016/j.gloplacha.2015.10.013

Chand P, Sharma MC, Bhambri R, et al. (2017) Reconstructing the pattern of the Bara Shigri Glacier fluctuation since the end of the Little Ice Age, Chandra valley, north-western Himalaya. Prog Phys

Geogr 41(5):643–675. https://doi.org/10.1177/0309133317728017

Das S, Sharma MC (2019) Glacier changes between 1971 and 2016 in the Jankar Chhu Watershed, Lahaul Himalaya, India. J Glaciol 65(249):13–28. https://doi.org/10.1017/jog.2018.77

Dehecq A, Gourmelen N, Gardner AS, et al. (2019) Twenty-first century glacier slowdown driven by mass loss in High Mountain Asia. Nat Geosci 12:22–27. https://doi.org/10.1038/s41561-018-0271-9

Farinotti D, Huss M, Fürst JJ, et al. (2019) A consensus estimate for the ice thickness distribution of all glaciers on Earth. Nat Geosci 12:168–173. https://doi.org/10.1038/s41561-019-0300-3

Fitzgerald RW, Lees BG (1994) Assessing the classification accuracy of multisource remote sensing data. Remote Sens Environ 47(3):362–368. https://doi.org/10.1016/0034-4257(94)90103-1

Fujita K, Ageta Y (2000) Effect of summer accumulation on glacier mass balance on the Tibetan Plateau revealed by mass-balance model. J Glaciol 46(153):244–252. https://doi.org/10.3189/172756500781832945

Gaddam VK, Sharma P, Patel LK, et al. (2016) Spatio-temporal changes observed in supra-glacial debris cover in Chenab basins, Western Himalaya. Proc. of SPIE 9878:98781F. https://doi.org/10.1117/12.2227993

Garg PK, Shukla A, Tiwari RK, et al. (2017) Assessing the status of glaciers in part of the Chandra basin, Himachal Himalaya: a multiparametric approach. Geomorphology 284:99–114. https://doi.org/10.1016/j.geomorph.2016.10.022

Garg S, Navinkumar PJ, Godara A, et al. (2023) Remote sensing the evolution of debris-covered Panchi Nala-A glacier, India (1971-2021) from satellited and Unmanned Areial Vehicle. Region Environ Change 23:103. https://doi.org/10.1007/s10113-023-02096-1

Granshaw FD, Fountain AG (2006) Glacier change (1958-1998) in the North Cascades National Park Complex, Washington, USA. J Glaciol 52(177):251–256. https://doi.org/10.3189/172756506781828782

Gratton DJ, Howarth PJ, Marceau DJ (1990) Combining DEM parameters with Landsat MSS and TM imagery in a GIS for mountain glacier characterization. IEEE Trans Geosci Remote Sens 28(4):766–769. https://doi.org/10.1109/TGRS.1990.573023

Haeberli W, Hoelzle M (1995) Application of inventory data for estimating characteristics of and regional climate-change effects on mountain glaciers: a pilot study with the European Alps. Ann Glaciol 21:206–212. https://doi.org/10.3189/s0260305500015834

Hall DK, Bayr KJ, Schöner W, et al. (2003) Consideration of the errors inherent in mapping historical glacier positions in Austria from the ground and space (1893-2001). Remote Sens Environ 86(4):566–577. https://doi.org/10.1016/S0034-4257(03)00134-2

Hersbach H, Bell B, Berrisford P, et al. (2020) The ERA5 global reanalysis. RMetS 146(730):1999-2049. https://doi.org/10.1002/qj.3803

Herreid S, Pellicciotti F, Ayala A, et al. (2015) Satellite observations show no net change in the percentage of supraglacial debris-covered area in northern Pakistan from 1977 to 2014. J Glaciol 61(227):524–536. https://doi.org/10.3189/2015JoG14J227

Hocking R (1976) The analysis and selection of variables in linear regression. Biometrics 32(1): 1–49. https://doi.org/10.2307/2529336

Holobâcă IH, Tielidze LG, Ivan K, et al. (2021) Multi-sensor remote sensing to map glacier debris cover in the Greater Caucasus, Georgia. J Glaciol 67(264):685-696. https://doi.org/10.1017/jog.2021.47

Huang L, Li Z, Zhou JM, et al. (2021) An automatic method for clean glacier and nonseasonal snow area change estimation in High Mountain Asia from 1990 to 2018. Remote Sens Environ:. 258:112376. https://doi.org/10.1016/j.rse.2021.112376

Hugonnet R, McNabb R, Berthier E, et al. (2021) Accelerated global glacier mass loss in the early twenty-first century. Nature 592:726–731. https://doi.org/10.1038/s41586-021-03436-z

Ismail MH, Jusoff K (2008) Satellite data classification accuracy assessment based from reference dataset. World Acad Sci, Engi Techn, Int J Environ, Chem, Eco, Geol Geophys Engin 2 :23 – 29. https://api.semanticscholar.org/CorpusID:9169350

Janssen LLF,van der Wel FJM (1994) Accuracy assessment of satellite derived land-cover data: a review. Photogramm Eng Remote Sens 60:419–426. https://www.osti.gov/biblio/6448244

Jin R, Li X, Che T, et al. (2005) Glacier area changes in the Pumqu river basin, Tibetan Plateau, between the 1970s and 2001. J Glaciol 51(125):607–610. https://doi.org/10.3189/172756505781829061

Kääb A (2002) Monitoring high-mountain terrain deformation from repeated air and spaceborne optical data: examples using digital aerial imagery and ASTER data. ISPRS J Photogramm Remote Sens 57(1-2):39–52. https://doi.org/10.1016/S0924-2716(02)00114-4

Kaushik S, Dharpure JK, Joshi PK, et al. (2020) Climate change drives glacier retreat in Bhaga basin located in Himachal Pradesh, India. Geocarto Int 35(11): 1179-1198. https://doi.org/10.1080/10106049.2018.1557260

King O, Dehecq A, Quincey D, et al. (2018) Contrasting geometric and dynamic evolution of lake and land-terminating glaciers in the central Himalaya. Glob Planet Change 167:46–60. https://doi.org/10.1016/j.gloplacha.2018.05.006

Kulkarni AV, Shirsat TS, Kulkarni A, et al. (2021) State of Himalayan cryosphere and implications for water security. Water Secur 14:100101. https://doi.org/10.1016/j.wasec.2021.100101

Kulkarni AV, Rathore BP, Singh SK, et al. (2011) Understanding changes in the Himalayan cryosphere using remote sensing techniques. Int J Remote Sens 32(3): 601-615. https://doi.org/10.1080/01431161.2010.517802

Kulkarni AV, Bahuguna IM, Rathore BP, et al. (2007) Glacial retreat in Himalaya using Indian Remote Sensing satellite data. Curr Sci 92:69–74. https://www.jstor.org/stable/24096824

Kumar A, Mishra R, Chitranshi A (2015) Long term monitoring of mass balance of Hamtah Glacier, Lahaul and Spiti district, Himachal Pradesh. J Ind Geophy Union 19:414-421.

Li F, Maussion F, Wu G, et al. (2022) Influence of glacier inventories on ice thickness estimates and future glacier change projections in the Tian Shan range, Central Asia. J. Glaciol 69(274):266-280. https://doi.org/10.1017/jog.2022.60

Mandal A, Ramanathan A, Azam MF, et al. (2020) Understanding the interrelationships among mass balance, meteorology, discharge and surface velocity on Chhota Shigri Glacier over 2002-2019 using in situ measurements. J Glaciol 66(259):727–741. https://doi.org/10.1017/jog.2020.42

Maurer JM, Rupper SB, Schaefer JM (2016) Quantifying ice loss in the eastern Himalayas since 1974 using declassified spy satellite imagery. The Cryosphere 10(5):2203–2215. https://doi.org/10.5194/tc-10-2203-2016

Ismail MH, Jusoff K (2008) Satellite data classification accuracy assessment based from reference dataset. World Acad Sci Eng Tech 2:23-29. https://api.semanticscholar.org/CorpusID:9169350

Mölg N, Bolch T, Rastner P, et al. (2018) A consistent glacier inventory for Karakoram and Pamir derived from Landsat data: distribution of debris cover and mapping challenges. Earth Syst Sci Data 10(4):1807–1827. https://doi.org/10.5194/essd-10-1807-2018

Muhammad S, Thapa A (2020) An improved Terra-Aqua MODIS snow cover and Randolph Glacier Inventory 6.0 combined product (MOYDGL06) for High Mountain Asia between 2002 and 2018. Earth Syst Sci Data 12(1):345–356. https://doi.org/10.5194/essd-12-345-2020

Mukherjee K, Bhattacharya A, Pieczonka T, et al. (2018) Glacier mass budget and climate reanalysis data indicate a climatic shift around 2000 in Lahaul-Spiti, western Himalaya. Clim Change 148:219–233. https://doi.org/10.1007/s10584-018-2185-3

Nela BR, Singh G, Bandyopadhyay D, et al. (2020) Estimating dynamic parameters of Bara Shigri Glacier and derivation of mass balance from velocity. Int Geosci Remote Sens Symp 3002–3005. https://doi.org/10.1109/IGARSS39084.2020.9323152

Oliphant AJ, Spronken-Smith RA, Sturman AP, et al. (2003) Spatial variability of surface radiation fluxes in mountainous terrain. J Appl Meteorol 42:113–128. https://doi.org/10.1175/1520-0450(2003)042<0113:SVOSRF>2.0.CO;2

Oulkar SN, Thamban M, Sharma P, et al. (2022) Energy fluxes, mass balance, and climate sensitivity of the Sutri Dhaka Glacier in the western Himalaya. Front Earth Sci 10: 949735. https://doi.org/10.3389/feart.2022.949735

Pai DS, Sridhar L, Rajeevan M, et al. (2014) Development of a new high spatial resolution (0.25° X 0.25°) Long period (1901-2010) daily gridded rainfall data set over India and its comparison with existing data sets over the region. MAUSAM 65; 1-18. http://www.imdpune.gov.in (Accessed 24 December 2023)

Pandey P, Venkataraman G (2013) Changes in the glaciers of Chandra–Bhaga basin, Himachal Himalaya, India, between 1980 and 2010 measured using remote sensing. Int J Remote Sens 34(15):5584–5597. https://doi.org/10.1080/01431161.2013.793464

Patel LK, Sharma A, Sharma P, et al. (2021) Glacier area changes and its relation to climatological trends over western Himalaya between 1971 and 2018. J Earth Syst Sci 130:1-15. https://doi.org/10.1007/s12040-021-01720-0

Patel LK, Sharma P, Fathima TN, et al. (2018) Geospatial observations of topographical control over the glacier retreat, Miyar basin, western Himalaya, India. Environ Earth Sci 77:1–12. https://doi.org/10.1007/s12665-018-7379-5

Paul F (2000) Evaluation of different methods for glacier mapping using landsat TM. Proc EARSeL-SIG-Workshop L Ice Snow, Dresden/FRG 239–245. http://www.glims.org/algorithms/paul_lis_02.PDF (Accessed on 10 December 2019)

Paul F, Bolch T, Briggs K, et al. (2017) Error sources and guidelines for quality assessment of glacier area, elevation change, and velocity products derived from satellite data in the Glaciers_cci project. Remote Sens Environ 203:256–275. https://doi.org/10.1016/j.rse.2017.08.038

Paul F, Bolch T, Kääb A, et al. (2015) The glaciers climate change initiative: methods for creating glacier area, elevation change and velocity products. Remote Sens Environ 162:408–426. https://doi.org/10.1016/j.rse.2013.07.043

Paul F, Barrand NE, Baumann S, et al. (2013) On the accuracy of glacier outlines derived from remote-sensing data. Ann Glaciol 54(63):171–182. https://doi.org/10.3189/2013AoG63A296

Paul F, Frey H, Bris R Le (2011) A new glacier inventory for the European Alps from Landsat TM scenes of 2003: challenges and results. Ann Glaciol 52(59):144–152. https://doi.org/10.3189/172756411799096295

Paul F, Huggel C, Kääb A (2004) Combining satellite multispectral image data and a digital elevation model for mapping debris-covered glaciers. Remote Sens Environ 89(4):510–518. https://doi.org/10.1016/j.rse.2003.11.007

Paul F, Kääb A, Maisch M, et al. (2002) The new remote-sensing-derived Swiss glacier inventory: II. First results. Ann Glaciol 34(34):362–366. https://doi.org/10.3189/172756402781817473

Pfeffer WT, Arendt AA, Bliss A, et al. (2014) The randolph glacier inventory: A globally complete inventory of glaciers. J Glaciol 60(221):537–552. https://doi.org/10.3189/2014JoG13J176

Racoviteanu AE, Arnaud Y, Williams MW, et al. (2008) Decadal changes in glacier parameters in the Cordillera Blanca, Peru, derived from remote sensing. J Glaciol 54(186):499–510. https://doi.org/10.3189/002214308785836922

Racoviteanu AE, Paul F, Raup B, et al. (2009) Challenges and recommendations in mapping of glacier parameters from space: results of the 2008 global land ice measurements from space (GLIMS) workshop, Boulder, Colorado, USA. Ann Glaciol 50 (53):53-69. https://doi:10.3189/172756410790595804

Racoviteanu AE, Arnaud Y, Williams MW, et al. (2015) Spatial patterns in glacier characteristics and area changes from 1962 to 2006 in the Kanchenjunga-Sikkim area, eastern Himalaya. The Cryosphere 9(2):505–523. https://doi.org/10.5194/tc-9-505-2015

Racoviteanu AE, Rittger K, and Armstrong R (2019) An automated approach for estimating snowline altitudes in the Karakoram and eastern Himalaya from remote sensing. Front Earth Sci 7:220. https://doi.org/10.3389/feart.2019.00220

Ramsankaran R, Pandit A, Azam MF (2018) Spatially distributed ice-thickness modelling for Chhota Shigri Glacier in western Himalayas, India. Int J Remote Sens 39(10):3320–3343. https://doi.org/10.1080/01431161.2018.1441563

Rathore BP, Bahuguna I, Singh SK, et al. (2022) Monitoring snow cover in the Himalayan–Karakoram basins using AWiFS data: significant outcomes. Curr Sci 122(11):1305–1314. https://doi.org/10.18520/cs/v122/i11/1305-1314

RGI Consortium (2017) Randolph Glacier Inventory - a dataset of global glacier outlines, version 6. Boulder, Colorado USA. NSIDC: National Snow and Ice Data Center. https://doi.org/10.7265/4m1f-gd79

Sahu R, Gupta RD (2020) Glacier mapping and change analysis in Chandra basin , western Himalaya , India during 1971 – 2016. Int J Remote Sens 41(18):6914–6945. https://doi.org/10.1080/01431161.2020.1752412

Sakai A (2019) Brief Communication: Updated GAMDAM glacier inventory over the High Mountain Asia. The Cryosphere 13(7):1–12. https://doi.org/10.5194/tc-2018-139

Sakai A, Nishimura K, Kadota T, et al. (2009) Onset of calving at supraglacial lakes on debris-covered glaciers of the Nepal Himalaya. J Glaciol 55(193):909–917. https://doi.org/10.3189/002214309790152555

Salerno F, Buraschi E, Bruccoleri G, et al. (2008) Glacier surface-area changes in Sagarmatha national park, Nepal, in the second half of the 20th century, by comparison of historical maps. J Glaciol 54(187):738–752. https://doi.org/10.3189/002214308786570926

Salerno F, Thakuri S, Tartari G, et al. (2017) Debris-covered glacier anomaly? Morphological factors controlling changes in the mass balance, surface area, terminus position, and snow line altitude of Himalayan glaciers. Earth Planet Sci Lett 471:19–31. https://doi.org/10.1016/j.epsl.2017.04.039

Sandarp (2023) South Asia newtwork on dams, rivers and people. https://sandrp.files.wordpress.com/2018/03/dams_on_chenab_how_many_are_too_many_dec2012.pdf (Accessed on 11 March 2024)

Sattar A, Allen S, Mergili M, et al. (2023) Modeling potential glacial lake outburst flood process chains and effects from artificial lake‐level lowering at Gepang Gath lake, Indian Himalaya. J Geophys Res Earth Surf 128(3): e2022JF006826. https://doi.org/10.1029/2022jf006826

Scherler D, Bookhagen B, Strecker MR (2011a) Spatially variable response of Himalayan glaciers to climate change affected by debris cover. Nat Geosci 4:156–159. https://doi.org/10.1038/ngeo1068

Scherler D, Bookhagen B, Strecker MR (2011b) Hillslope-glacier coupling: The interplay of topography and glacial dynamics in High Asia. J Geophys Res Earth Surf 116(F2):1–21. https://doi.org/10.1029/2010JF001751

Schmidt S, Nüsser M (2017) Changes of high altitude glaciers in the trans-himalaya of Ladakh over the past five decades (1969-2016). Geosci 7(2):27. https://doi.org/10.3390/geosciences7020027

Shean DE, Bhushan S, Montesano P, et al. (2020) A systematic, regional assessment of High Mountain Asia Glacier mass balance. Front Earth Sci 7:363. https://doi.org/10.3389/feart.2019.00363

Shugar DH, Jacquemart M, Shean D, et al. (2021) A massive rock and ice avalanche caused the 2021 disaster at Chamoli, Indian Himalaya. Science (80) 373(6552):300–306. https://doi.org/10.1126/science.abh4455

Shukla A, Garg S, Mehta M, et al. (2020) Temporal inventory of glaciers in the Suru sub-basin, western Himalaya: impacts of regional climate variability. Earth Syst Sci Data 12(2):1245–1265. https://doi.org/10.5194/essd-12-1245-2020

Shukla A, Gupta RP, Arora MK (2009) Estimation of debris cover and its temporal variation using optical satellite sensor data: a case study in Chenab basin, Himalaya. J Glaciol 55(191):444–452. https://doi.org/10.3189/002214309788816632

Shukla A, Qadir J (2016) Differential response of glaciers with varying debris cover extent: evidence from changing glacier parameters. Int J Remote Sens 37(11):2453–2479. https://doi.org/10.1080/01431161.2016.1176272

Sidjak RW, Wheate RD (1999) Glacier mapping of the Illecillewaet icefield, British Columbia, Canada, using Landsat TM and digital elevation data. Int J Remote Sens 20(2):273–284. https://doi.org/10.1080/014311699213442

Soheb M, Ramanathan A, Bhardwaj A, et al. (2022) Multitemporal glacier inventory revealing four decades of glacier changes in the Ladakh region. Earth Syst Sci Data 14(9):4171–4185. https://doi.org/10.5194/essd-14-4171-2022

Srivastava S, and Azam MF (2022) Functioning of glacierized catchments in Monsoon and Alpine regimes of Himalaya. J Hydro 609:127671. https://doi.org/10.1016/j.jhydrol.2022.127671

Tawde SA, Kulkarni AV, and Bala G (2017) An estimate of glacier mass balance for the Chandra basin, western Himalaya, for the period 1984–2012. Ann Glaciol 58(75pt2):99-109. https://doi.org/10.1017/aog.2017.18

Wang Y, Hou S, Liu Y (2009) Glacier changes in the Karlik Shan, eastern Tien Shan, during 1971/72-2001/02. Ann Glaciol 50(53):39–45. https://doi.org/10.3189/172756410790595877

Xiang Y, Yao T, Gao Y, et al. (2018) Retreat rates of debris-covered and debris-free glaciers in the Koshi River Basin, central Himalayas, from 1975 to 2010. Environ Earth Sci 77(285):1–13. https://doi.org/10.1007/s12665-018-7457-8

Yan L, Wang J, Hao X, et al. (2014) Glacier mapping based on rough set theory in the Manas River watershed. Adv Sp Res 53(7):1071–1080. https://doi.org/10.1016/j.asr.2013.12.038

Yellala A, Kumar V, Høgda KA (2019) Bara Shigri and Chhota Shigri glacier velocity estimation in western Himalaya using Sentinel-1 SAR data. Int J Remote Sens 40(15):5861–5874. https://doi.org/10.1080/01431161.2019.1584685

Zalazar L, Ferri L, Castro M, et al. (2020) Spatial distribution and characteristics of Andean ice masses in Argentina: results from the first national glacier inventory. J Glaciol 66(260):938–949. https://doi.org/10.1017/jog.2020.55

Zhao X, Wang X, Wei J, et al. (2020) Spatiotemporal variability of glacier changes and their controlling factors in the Kanchenjunga region, Himalaya based on multi-source remote sensing data from 1975 to 2015. Sci Total Environ 745:140995. https://doi.org/10.1016/j.scitotenv.2020.140995

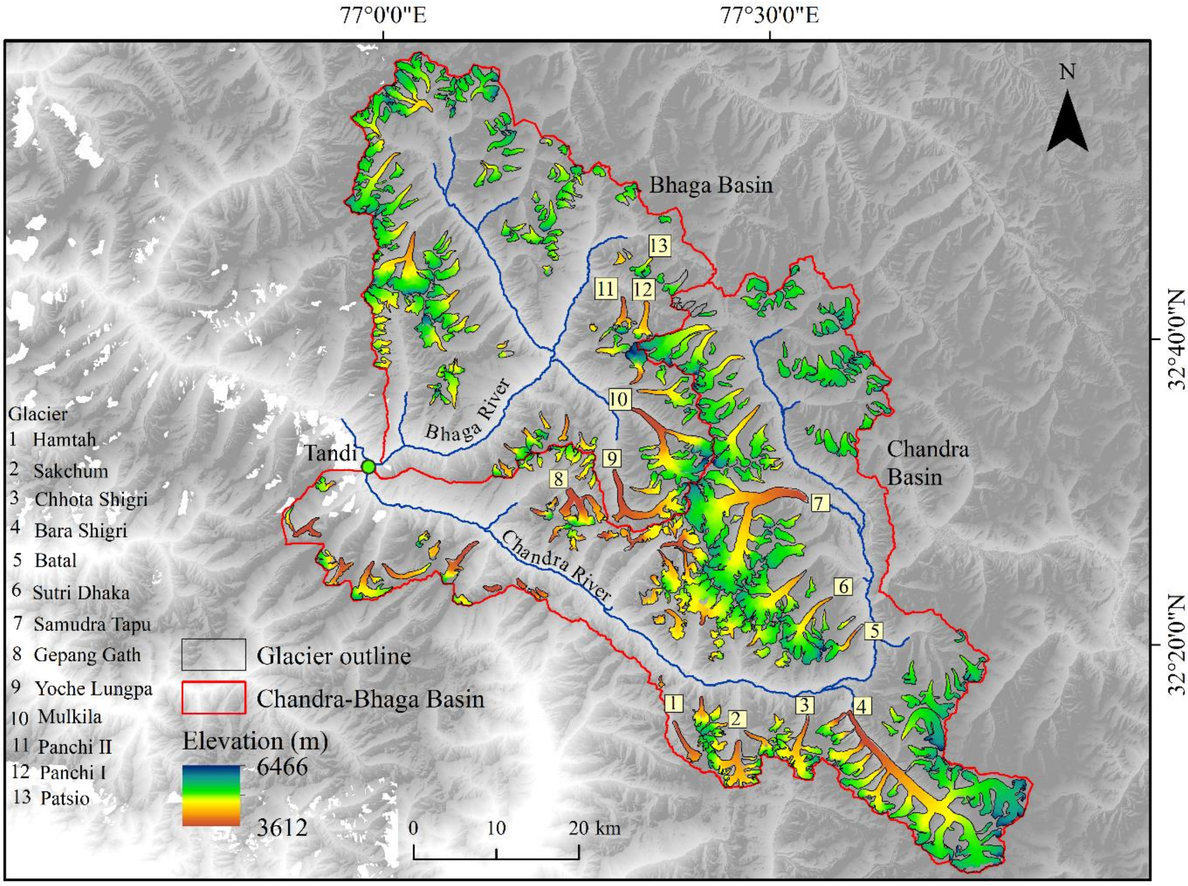

Fig. 1 Study area map of the Chandra-Bhaga Basin. Background image is hillshade using Shuttle Radar Topography Mission (SRTM) DEM with a spatial resolution of 30 m. Glacier boundaries used are from the present study.

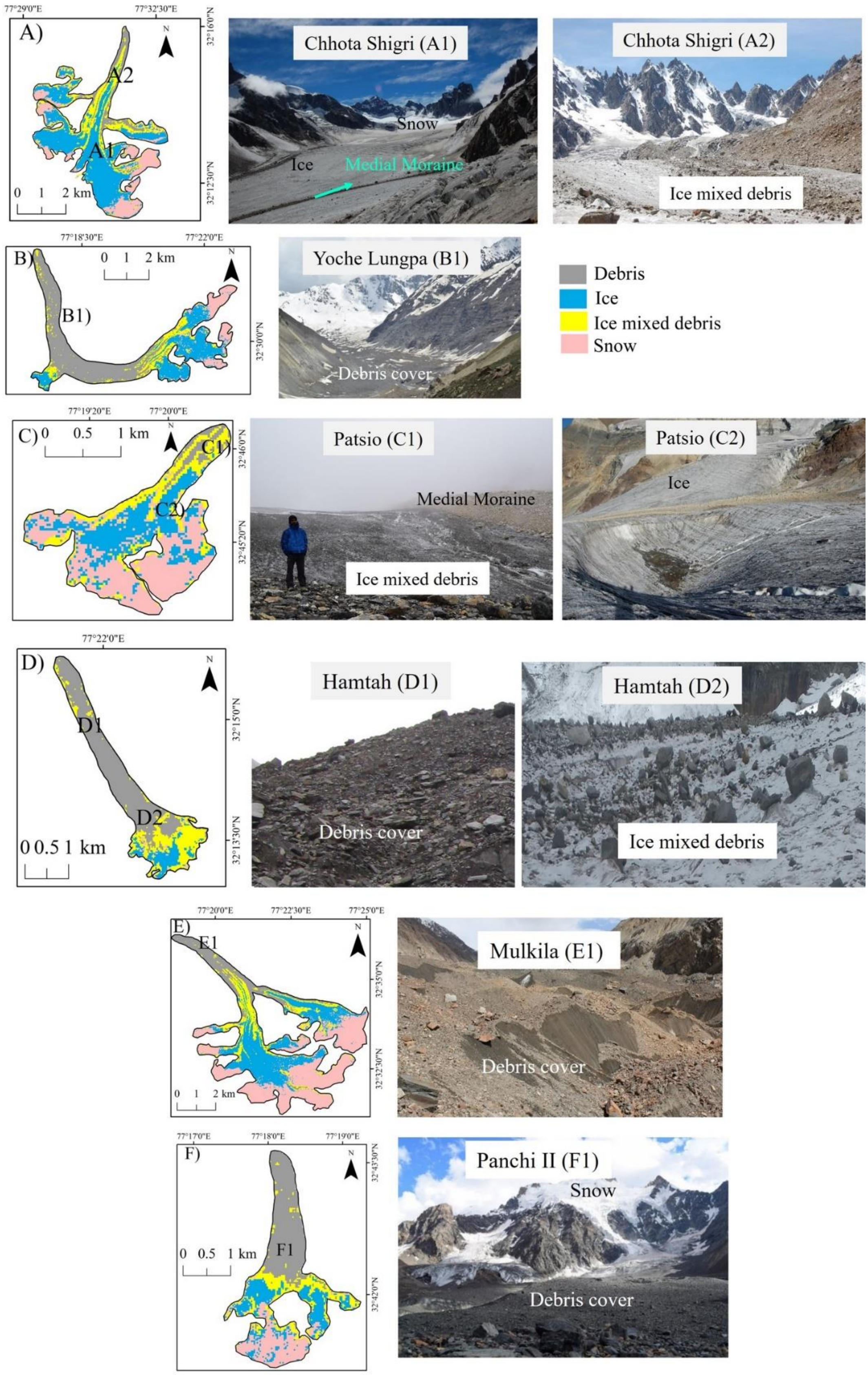
A)
A1
A2
0 1 2 km
N
77°29'0"E
77°32'30"E
32°16'0"N
32°12'30"N
Chhota Shigri (A1)
Snow
Ice
Medial Moraine
Chhota Shigri (A2)
Ice mixed debris
B)
B1)
0 1 2 km
77°18'30"E
77°22'0"E
32°30'0"N
Yoche Lungpa (B1)
Debris cover
Debris
Ice
Ice mixed debris
Snow
C)
0 0.5 1 km
C1)
C2)
77°19'20"E
77°20'0"E
32°46'0"N
32°45'20"N
Patsio (C1)
Medial Moraine
Ice mixed debris
Patsio (C2)
Ice
D)
D1
D2
0 0.5 1 km
77°22'0"E
32°15'0"N
32°13'30"N
Hamtah (D1)
Debris cover
Hamtah (D2)
Ice mixed debris
E)
E1
0 1 2 km
77°20'0"E
77°22'30"E
77°25'0"E
32°35'0"N
32°32'30"N
Mulkila (E1)
Debris cover
F)
F1
0 0.5 1 km
77°17'0"E
77°18'0"E
77°19'0"E
32°43'30"N
32°42'0"N
Panchi II (F1)
Snow
Debris cover

Fig. 2 Field photographs (in the right panel) for validation and classified Landsat images showing snow, ice, debris and ice mix debris cover. A) Yoche Lungpa Glacier, B) Patsio Glacier, C) Panchi II Glacier, D) Hamtah Glacier, E) Mulkila Glacier, F) Chhota Shigri Glacier.

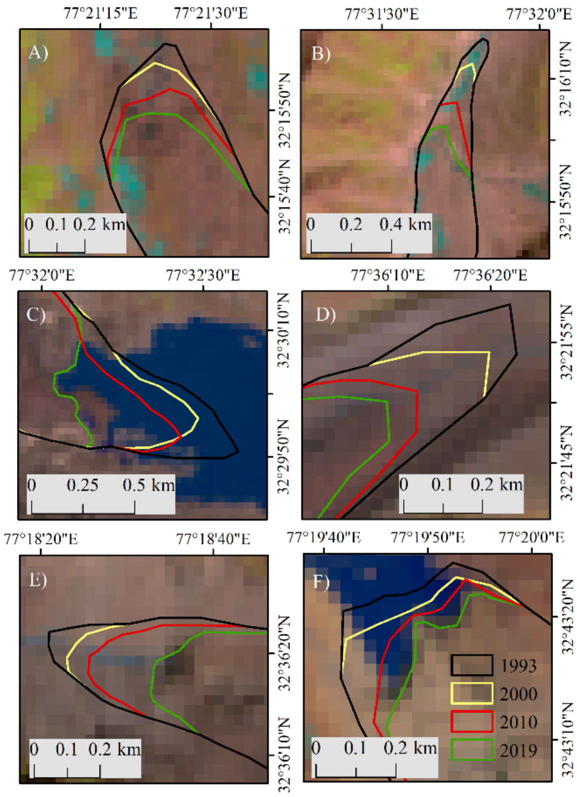

Fig. 3 Decadal retreat of the glaciers in Chandra-Bhaga Basin. A) Hamtah, B) Chhota Shigri, C) Samudra Tapu, D) Batal, E) Mulkila, F) Panchi I. Background image is a 2019 Landsat 8 OLI composite of bands 5, 4 and 3.

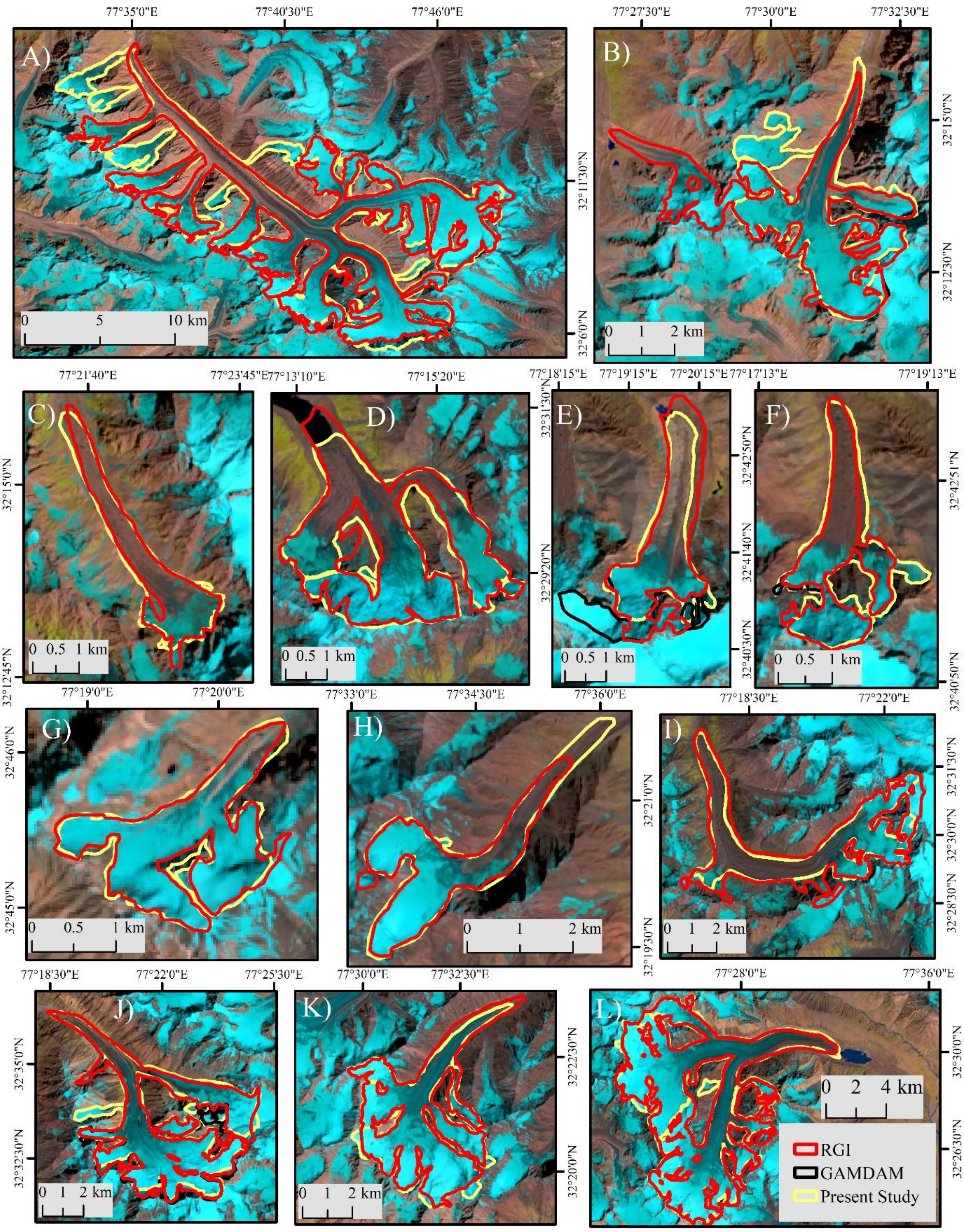

Fig. 4 Comparison of RGI 6.0 (red) (RGI Consortium 2017), GAMDAM (black) (Sakai 2019), and present glacier outlines (yellow) for A) Bara Shigri, B) Chhota Shigri, C) Hamtah, D) Gepang Gath, E) Panchi I, F) Panchi II, G) Patsio, H) Batal, I) Yoche Lungpa, J) Mulkila, K) Sutri Dhaka, and L) Samudra Tapu glaciers. Background image 2019 Landsat 8 OLI.

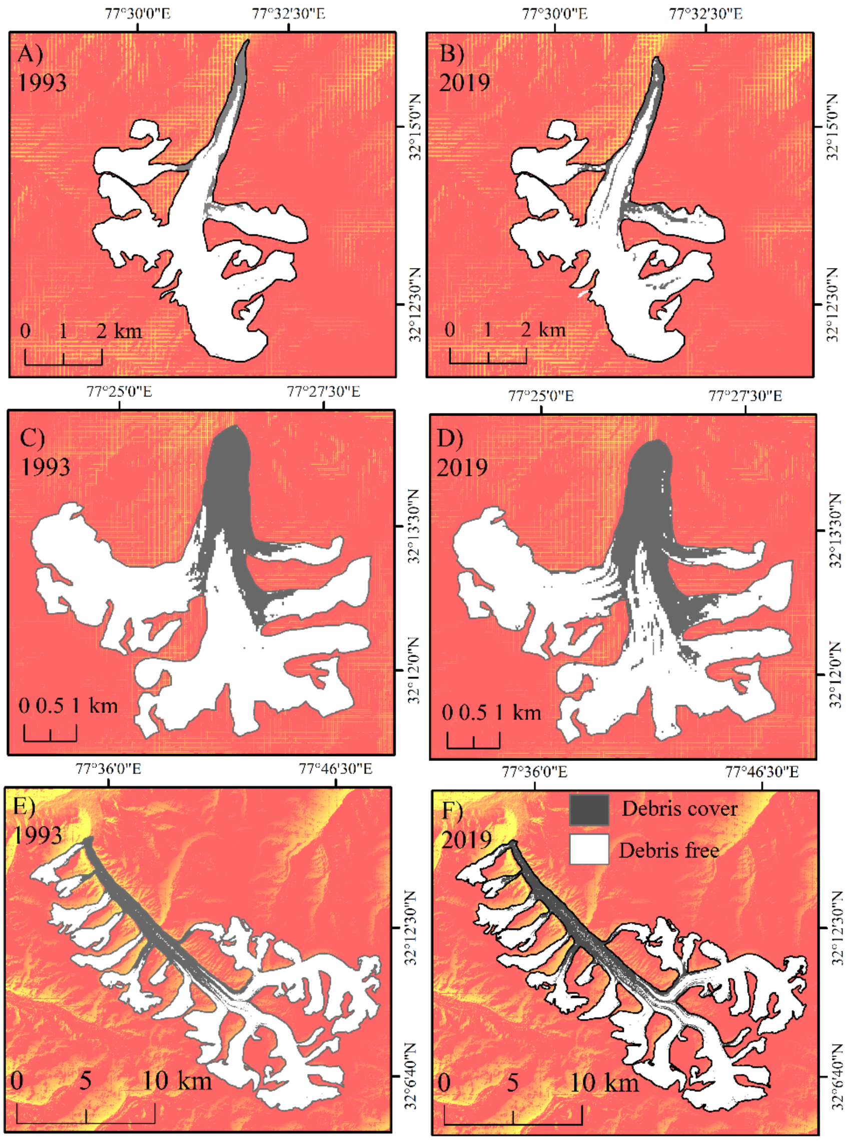

Fig. 5 SDC on the A) Chhota Shigri, C) Sakchum, and E) Bara Shigri glaciers. Background image is the hillshade of SRTM DEM.

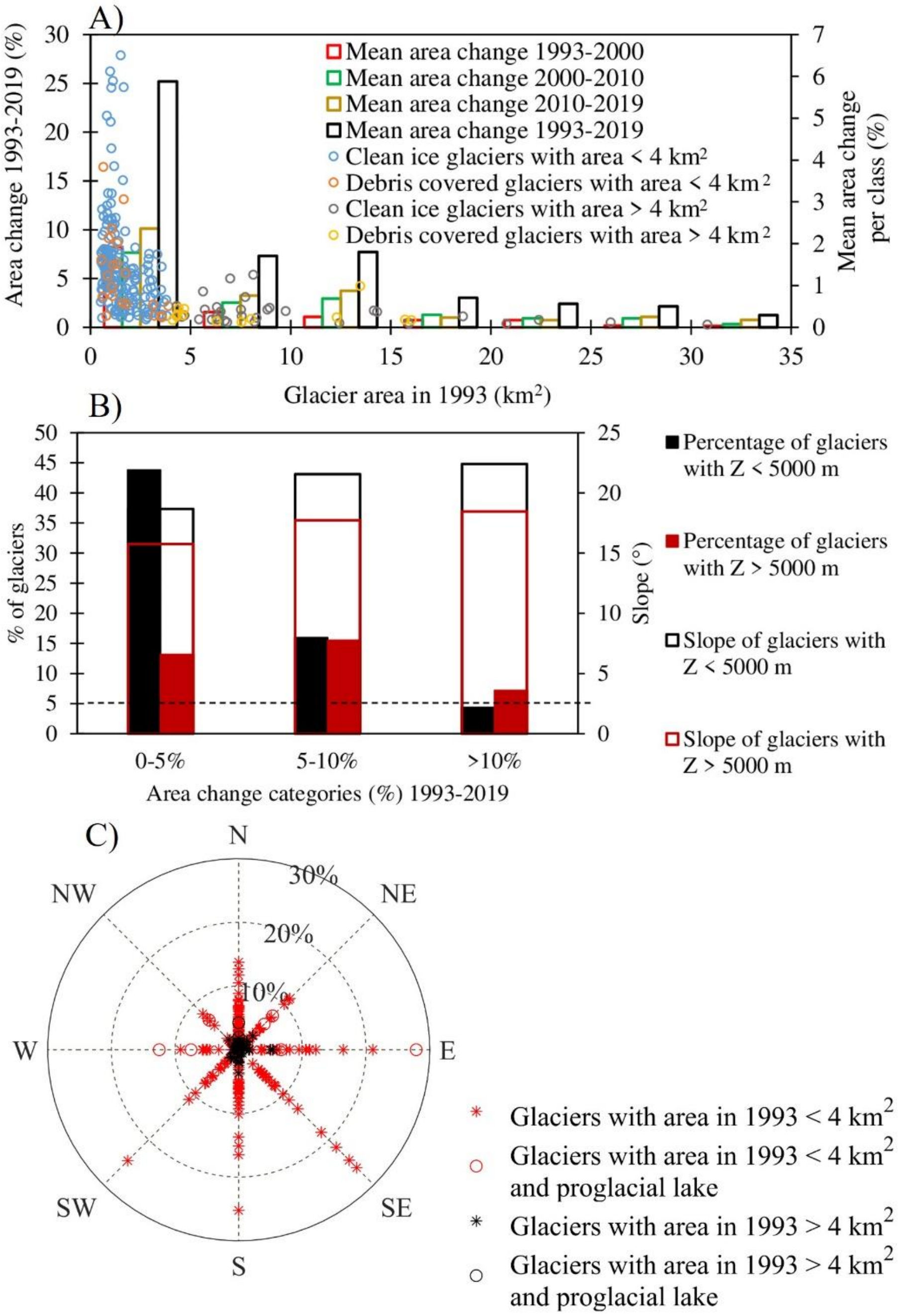

Fig. 6 (A) Area change (%) in debris-covered and clean ice glaciers plotted as a function of glacier area in 1993 (scatter), and mean glacier area change (%) for each glacier area class at specific time intervals (bars). (B) Percentage of glaciers and mean slope corresponding to minimum elevation (Z) < or > 5000 and for different area change categories. (C) Aspect and area change (%) for glacier area in 1993 < or > 4 km² and presence/absence of proglacial lake.

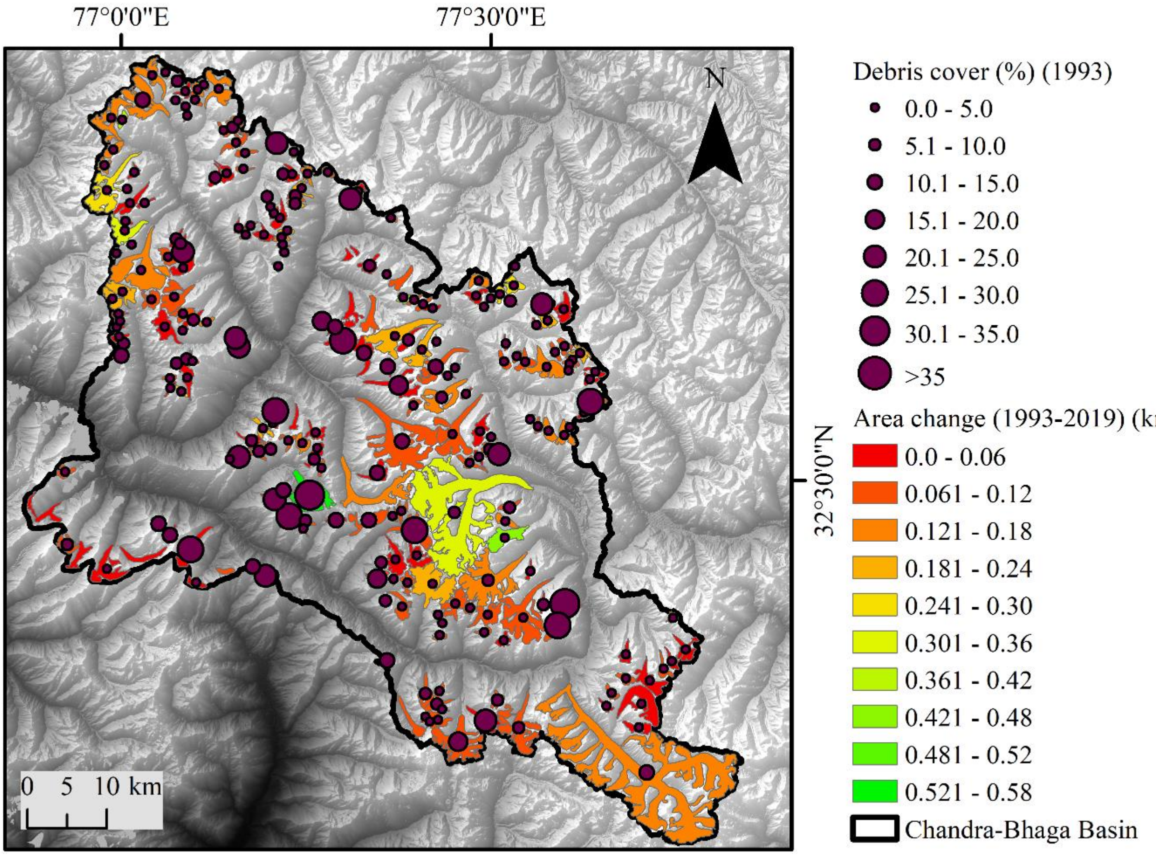

Fig. 7 Area change (1993 – 2019) of the glaciers in the Chandra-Bhaga Basin and its comparison to the percentage debris cover on the glacier in 1993. Background image is the hillshade effect of SRTM DEM.

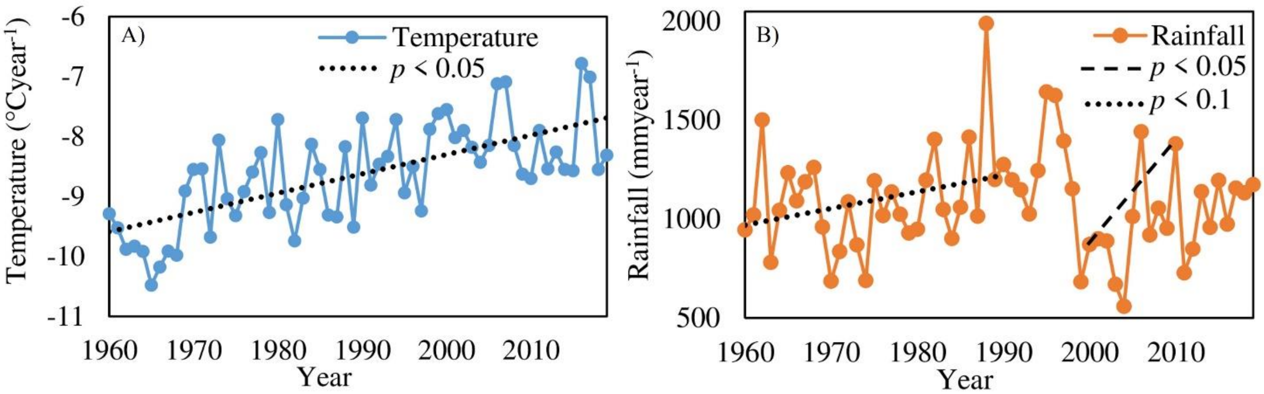

Fig. 8 Yearly time series of (A) 2 m air temperature (°C year⁻¹), (B) Rainfall (mm year⁻¹) in the Chandra-Bhaga Basin.

Table 1 Accuracy assessment matrix between field observations (columns) and remotely classified (rows) ground validation points for each category (debris, ice, ice mixed debris, and snow).

Class	Debris	Ice	Ice mixed debris	Snow	Total
Debris	39	0	2	0	41
Ice	0	44	3	2	49
Ice mixed debris	0	6	27	0	33
Snow	0	2	0	29	31
Total	39	52	32	31	154

Table 2 Change in the glacier area in Chandra-Bhaga Basin and the uncertainties associated.

Year	1993	2000	2010	2019
Total Area ± cumulative uncertainty (km²)	996 ± 62	989 ± 68	982 ± 66	973 ± 70
Total Area ± mean uncertainty (km²)	996 ± 0.5	989 ± 0.7	982 ± 0.5	973 ± 0.8
Period	1993-2000	2000-2010	2010-2019	1993-2019
Area change ± cumulative uncertainty (km²)	7 ± 6	7 ± 6	9 ± 8	23 ± 8
Area change ± mean uncertainty (km²)	7 ± 0.2	7 ± 0.2	9 ± 0.3	23 ± 0.3

Table 3 Decadal changes in the glacier area over some of the well-studied glaciers in the Chandra-Bhaga Basin.

Glacier	Area change (km²)			Glacier area 2019 (km²)
	1993-2000	2000-2010	2010-2019	
Hamtah	0.02±0.001	0.03±0.002	0.04±0.002	3.80±0.45
Sakchum	0.02±0.001	0.04±0.001	0.06±0.003	15.93±1.63
Chhota Shigri	0.02±0.001	0.12±0.002	0.18±0.001	15.47±0.85
Bara Shigri	0.10±0.021	0.06±0.003	0.11±0.014	131.47±9.54
Batal	0.03±0.002	0.03±0.001	0.04±0.002	4.59±0.53
Sutri Dhaka	0.02±0.001	0.05±0.001	0.20±0.003	20.50±0.90
Samudra Tapu	0.02±0.005	0.04±0.001	0.11±0.007	81.68±5.10
Gepang Gath	0.08±0.004	0.14±0.008	0.30±0.020	12.90±0.98
Yoche Lungpa	0.04±0.001	0.07±0.002	0.11±0.002	15.58±1.45
Mulkila	0.01±0.001	0.03±0.001	0.06±0.003	30.72±2.35
Panchi II	0.01±0.001	0.02±0.001	0.03±0.002	4.27±0.55
Panchi I	0.01±0.001	0.03±0.002	0.04±0.002	4.33±0.45
Patsio	0.02±0.001	0.04±0.001	0.09±0.001	2.75±0.20

Table 4 Surface Debris Cover (SDC) of representative glaciers (marked in Fig. 1) of the basin for the years 1993 and 2019.

S. No. (As in Fig.1)	Glacier	SDC (km^2)		SDC change (km^2)	Debris cover (% glacier area)	
		1993	2019		1993	2019
1	Hamtah	2.25 ± 0.41	2.32 ± 0.42	0.07 ± 0.01	59	62
2	Sakchum	2.80 ± 0.50	3.80 ± 0.68	1.00 ± 0.18	18	24
3	Chhota Shigri	1.45 ± 0.26	2.16 ± 0.39	0.71 ± 0.13	8	12
4	Bara Shigri	18.46 ± 3.32	23.40 ± 4.21	4.94 ± 0.89	14	18
5	Batal	1.17 ± 0.21	1.19 ± 0.21	0.02 ± 0.01	25	27
6	Sutri Dhaka	0.24 ± 0.04	0.53 ± 0.09	0.29 ± 0.05	1	2
7	Samudra Tapu	5.53 ± 1.01	8.49 ± 1.52	2.96 ± 0.53	6	10
8	Gepang Gath	4.34 ± 0.78	4.47 ± 0.80	0.13 ± 0.03	30	30
9	Yoche Lungpa	6.55 ± 1.17	6.90 ± 1.24	0.35 ± 0.06	42	45
10	Mulkila	3.51 ± 0.63	4.28 ± 0.77	0.77 ± 0.14	11	14
11	Panchi II	1.66 ± 0.30	1.67 ± 0.31	0.01 ± 0.01	39	40
12	Panchi I	1.86 ± 0.33	1.87 ± 0.34	0.01 ± 0.01	42	44
13	Patsio	0.17 ± 0.03	0.17 ± 0.03	0.00 ± 0.00	6	6

Table 5 SDC variation of some glaciers in Chandra-Bhaga Basin.

Glacier	SDC (km^2)		SDC (% glacier area)		Area (km^2)	
	1993	2019	1993	2019	1993	2019
Chhota Shigri	1.45	2.16	8	12	15.78±0.86	15.47±0.85
Hamtah	2.25	2.32	59	62	3.89±0.47	3.80±0.45
Panchi II	1.66	1.67	39	40	4.33±0.56	4.27±0.55
Panchi I	1.86	1.87	42	44	4.41±0.43	4.33±0.45
Bara Shigri	18.46	23.40	14	18	131.73±9.57	131.47±9.54
Patsio	0.17	0.17	6	6	2.89±0.20	2.75±0.20
Mulkila	3.51	4.28	11	14	30.81±1.83	30.72±2.35
Yoche Lungpa	6.55	6.90	42	45	15.71±1.45	15.58±1.45
Sakchum	2.80	3.80	18	24	16.04±1.64	15.93±1.63
Batal	1.17	1.19	25	27	4.68±0.55	4.59±0.53
Sutri Dhaka	0.24	0.53	1	2	20.77±0.91	20.50±0.90
Samudra Tapu	5.53	8.49	6	10	82.46±5.07	81.68±5.1
Gepang Gath	4.47	4.34	30	30	13.48±1.05	12.90±0.98

Table 6 Result of multivariate linear regression model to understand the spatiotemporal change variability of Chandra-Bhaga Basin glaciers.

Variables	Coefficient associated	p
Minimum elevation	0.001	0.9
Glacier size	-0.002	< 0.05
Aspect	0.06	<0.4
Slope	-0.12	< 0.05
SDC	-0.01	0.1
R^2	0.12	

Note: The variables have been standardized, making the coefficients directly representative of their relative influence on the glacier area change variability.

Appendix 1 List of Landsat and DEM datasets used for inventory and SDC change estimation of the glaciers.

Sensor/Map	Path/Row	Scene/Product ID	Acquisition Date	Spatial Resolution	Temporal Resolution
LANDSAT 5 (TM)	147 / 37	LT51470371992227ISP00	1992/08/14	VIS + MIR (30 m)	16 days
LANDSAT 5 (TM)	147 / 38	LT51470381992227ISP00	1992/08/14	VIS + MIR (30 m)	16 days
LANDSAT 5 (TM)	147 / 37	LT51470371993229ISP00	1993/08/17	VIS + MIR (30 m)	16 days
LANDSAT 5 (TM)	147 / 38	LT51470381993229ISP00	1993/08/17	VIS + MIR (30 m)	16 days
LANDSAT 7 (ETM)	147 / 37	LE71470372000289SGS00	2000/10/15	VIS + MIR (30 m)	16 days
LANDSAT 7 (ETM)	147 / 38	LE71470382000289SGS00	2000/10/15	VIS + MIR (30 m)	16 days
LANDSAT 5 (TM)	147 / 37	LT51470372011295KHC00	2011/11/22	VIS + MIR (30 m)	16 days
LANDSAT 5 (TM)	147 / 38	LT51470382011295KHC00	2011/10/22	VIS + MIR (30 m)	16 days
LANDSAT 5 (TM)	147 / 38	LT51470382010276KHC00	2011/11/30	VIS + MIR (30 m)	16 days
LANDSAT 7 (ETM)	147 / 37	LE71470372010284ASN00	2010/10/11	VIS + MIR (30 m)	16 days
LANDSAT 7 (ETM)	147 / 38	LE71470382010284ASN00	2010/10/11	VIS + MIR (30 m)	16 days
LANDSAT 8(OLI)	147 / 37	LC81470372019253LGN00	2019/09/10	VIS + MIR (30 m)	16 days
LANDSAT 8(OLI)	147 / 38	LC81470382019253LGN00	2019/09/10	VIS + MIR (30 m)	16 days
SRTM DEM	-	-	2000	30m	-

Note: TM represents thematic mapper; ETM represents enhanced thematic mapper; VIS means visible; MIR means mid infra-red.